The Islamic University–Gaza
Research and Postgraduate Affairs
Faculty of Science
Department of Physics

الجامعـــــــة الإســـلاميـة – غـزة
شئون البحث العلمي والدراسات العليا
كليـــــــــــة العلـــــــــوم
قســـــــم الفيـزيـــــــــــاء

Nonlinear waveguide structure sensors containing Graphene

تركيبات مجسات من أدلة موجيةغير خطية تحتوي على الجرافين

Rana Amin Khalifa

Supervised by

Distinguished Professor Dr. Mohammed M. Shabat

Distinguished Professor of Theoretical Physics

A thesis submitted in partial fulfillment
Of the requirements for the degree of
Master of Science in Physics

April/2017

إقـــــرار

أنا الموقع أدناه مقدم الرسالة التي تحمل العنوان:

Nonlinear waveguide structure sensors containing Graphene

تركيبات مجسات من أدلة موجيةغير خطية تحتوي على الجرافين

أقر بأن ما اشتملت عليه هذه الرسالة إنما هو نتاج جهدي الخاص، باستثناء ما تمت الإشارة إليه حيثما ورد، وأن هذه الرسالة ككل أو أي جزء منها لم يقدم من قبل الآخرين لنيل درجة أو لقب علمي أو بحثي لدى أي مؤسسة تعليمية أو بحثية أخرى. وأن حقوق النشر محفوظة للجامعة الإسلامية – غزة.

Declaration

I hereby certify that this submission is the result of my own work, except where otherwise acknowledged, and that this thesis (or any part of it) has not been submitted for a higher degree or quantification to any other university or institution. All copyrights are reserves to IUG.

Student's name:	رنا أمين هاشم خليفة	اسم الطالب:
Signature:	رنا خليفة	التوقيع:
Date:	17/5/2017	التاريخ:

بسم الله الرحمن الرحيم

الجامعة الإسلامية غزة
The Islamic University of Gaza

مكتب نائب الرئيس للبحث العلمي والدراسات العليا هاتف داخلي 1150

الرقم: ج س غ/35/ Ref:

التاريخ: 13/05/2017 Date:

نتيجة الحكم على أطروحة ماجستير

بناءً على موافقة شئون البحث العلمي والدراسات العليا بالجامعة الإسلامية بغزة على تشكيل لجنة الحكم على أطروحة الباحثة/ **رنا امين هاشم خليفة** لنيل درجة الماجستير في **كلية العلوم** قسم **الفيزياء** وموضوعها:

مجسمات من أدلة موجية تحتوي على الجرافين

Nonlinear waveguide structure sensor containing Graphene

وبعد المناقشة العلنية التي تمت اليوم السبت 16 شعبان 1438هـ، الموافق 2017/05/13م الساعة الحادية عشر صباحاً، اجتمعت لجنة الحكم على الأطروحة والمكونة من:

أ.د. محمد موسى شبات	مشرفاً و رئيساً	.....
أ.د. هالة جارالله الخزندار	مناقشاً داخلياً	.....
أ.د. رفعة جارالله الخزندار	مناقشاً خارجياً	.....

وبعد المداولة أوصت اللجنة بمنح الباحثة درجة الماجستير في كلية العلوم/ قسم الفيزياء.

واللجنة إذ تمنحها هذه الدرجة فإنها توصيها بتقوى الله ولزوم طاعته وأن تسخر علمها في خدمة دينها ووطنها.

والله ولي التوفيق،،،

نائب الرئيس لشئون البحث العلمي والدراسات العليا

أ.د. عبدالرؤوف علي المناعمة

+97082644400 +97082644800 public@iugaza.edu.ps www.iugaza.edu.ps iugaza iugaza mediaiug iugaza
P.O Box 108, Rimal,Gaza,Palestine ص.ب 108 الرمال . غزة . فلسطين

Abstract

Graphene is a single layer of covalently bonded carbon atoms, which was discovered at the last decade. It has electronical transport and optical properties so that it is unusual material it yet has already attracted intense research.

In this work, a three layer waveguide sensor is proposed. The structure consists of an infinitesimally sheet of thin conducting graphene material layer which is followed by dielectric layer and a substrate layer of kerr-like nonlinear medium. The dispersion relation of such a structure is derived in terms of the thickness and the physical parameters. The dispersion relation for the waveguide structure for transverse electric (*TE*-Mode) wave and nonlinear equation were also investigated. The sensitivity of the effective refractive index to variations in the refractive index of the cladding is obtained. Sensitivity has been obtained by tuning some physical parameters.

This thesis has concluded that the proposed sensor gave results for the sensitivity. The results are very important and useful for the practical application of graphene-based optoelectronic sensors.

Keywords: Graphene, Nonlinear, Waveguides, Effective Index, Sensitivity, Sensors**.**

الملخص

الجرافين هو عبارة عن طبقة واحدة من ذرات الكربون المرتبطة تساهميا، والذي تم اكتشافه في العقد الماضي. والذي يتمتع بخاصية النقل الإلكتروني، ولديه أيضا خصائص بصرية لذا يعتبر مادة غير عادية و ما زالت تجذب الانتباه

في هذا العمل، تم تصميم مقترح لجهازاستشعار الدليل الموجي مكون من ثلاث طبقات. ويتكون الهيكل من طبقة رفيعة من مادة الجرافين الموصلة وتليها طبقة عازلة وطبقة غير خطية مثل kerr. تم اشتقاق علاقة التشتت في هذا الهيكل من حيث السماكة والمعايير الفيزيائية. وأيضا قد تم التحقق من العلاقة بين تشتت هيكل الدليل الموجي للامواج الكهربائية المستعرضة (*TE*-mode) والمعادلة غير الخطية. تم الحصول على حساسية معامل الانكسار الفعال للتغيرات في معامل انكسار الغلاف. وقد تم قياس الحساسية من خلال ضبط بعض المعايير الفيزيائية

وقد خلص هذا البحث الى أن جهاز الاستشعار المقترح أعطى نتائج للحساسية. وقد كانت النتائج مهمة جدا ومفيدة للتطبيق العملي في أجهزة الاستشعار الضوئية المبينة على الجرافين

الكلمات المفتاحية : الجرافين ، غير خطية ، مرشدات الموجات ، معامل الانكسار ، الحساسية ، المجسات .

Dedication

All praise to Allah, today we fold the days tiredness and the errand summing up between the cover of this humble work

To the utmost knowledge lighthouse, to our greatest and most honored prophet Mohamed - May peace and grace from Allah be upon him

To my loving and caring mother…

To my spirt father …

To my aunt…

To my sisters…

To my brother in low…

To the taste of the most beautiful moments with my friends

I guide this research

Rana Amin Khalifa

Acknowledgment

In the name of Allah, to whom I am overwhelmed with gratitude for his continuous help and guidance throughout the path of knowledge.

I would like to express my deep thanks to all people who were involved in helped me to undertake my study, without whose cooperation this study would not have been possible.

My deepest gratitude to *Professor Dr. Mohamed M. Shabat*, my supervisor, for his unbelievable support, I offer my warmest thanks and gratitude to him for his kind care, his intelligence and tolerance in academic supervision, continuous reassurance, motivation and friendly support .

I would like to thank my thesis committee memers Professor Dr. Hala J. El-Khozondar from Electrical Engineering department, IUG and Dr. Rifa J. El-Khozondar from Physics department, Al-Aqsa Univesity for their valuable comments, feedback and guidance.

In addition, I would like to exend my thanks to all members of the Physics Department at IUG.

Special thanks to Dina and khouloud for continuous support and for his cooperation, facilitation and continuous reassurance.

I will never forget my family who supported and encouraged me all over the period of study.

My high appreciation to all people who have participated in helping me to complete my study.

Researcher

Rana Amin Khalifa

Table of Contents

List of Figures

List of Abbreviations

1D	One dimensional
2D	Two-dimensional
nm	Nanometer
N	Surface Plasmons
TE	Transverse Electric
THz	Terra Hertz
TM	Transverse Magnetic
r	Nonlinear factor
TEM	Transverse Electromagnetic

Chapter 1

The Fundamental of optical waveguides and Maxwell's Equations

Chapter 1

The fundamental of optical waveguides and Maxwell's Equations

This chapter presents the background and fundamental concepts of electromagnetic fields and waveguides. It provides a brief review of Maxwell's equations, wave equation and refractive index. The concepts of nonlinear, TE polarizations and waveguide modes are also presented.

1.1 Maxwell's Equations

Maxwell's Equations are used to govern the behavior of electric and magnetic fields. A flow of electric current produces a magnetic field. The magnetic field produce an electric field. Maxwell's Equations show that separated charge (positive and negative) gives rise to an electric field which is varying in time because it gives rise to a propagating electric field, further giving rise to a propagating magnetic field. Maxwell was one of the first to determine the speed of propagation of electromagnetic (EM) waves which was the same as the speed of light - and hence to conclude that EM waves and visible light were really the same thing. (Jackson, 1999; Born & Wolf, 1999);

Maxwell's equations were written as follows:

$$\vec{\nabla} \cdot \vec{D} = \rho, \tag{1.1}$$

$$\vec{\nabla} \times \vec{E} = -\frac{\partial B}{\partial t}, \tag{1.2}$$

$$\vec{\nabla} \cdot \vec{B} = 0, \tag{1.3}$$

$$\vec{\nabla} \times \vec{H} = \vec{J} + \frac{\partial \vec{D}}{\partial t}. \tag{1.4}$$

where E and H are the electric and magnetic fields, respectively, D and B are the electric and magnetic flux densities, respectively, and ρ and J are the electric charge and the current densities, respectively.

For wave propagation in an isotopic medium without free charges and conduction current ($\rho = 0$, and $J = 0$).

Eqs. (1.1), (1.2), (1.3) and (1.4) become as:

$$\vec{\nabla} \cdot \vec{D} = 0, \tag{1.5}$$

$$\vec{\nabla} \times \vec{E} = -\frac{\partial \vec{B}}{\partial t}, \tag{1.6}$$

$$\vec{\nabla} \cdot \vec{B} = 0, \tag{1.7}$$

$$\vec{\nabla} \times \vec{H} = \frac{\partial \vec{D}}{\partial t}. \tag{1.8}$$

1.2 Constitutive Relations

The fields and flux densities in Eqs. (1.5), (1.6), (1.7) and (1.8) are related to each other by the constitutive relations. For a linear, isotropic, homogeneous medium the constitutive relations can be written as:

$$\vec{D} = \varepsilon \vec{E}, \tag{1.9}$$

$$\vec{B} = \mu \vec{H}, \tag{1.10}$$

$$\vec{J} = \sigma \vec{E}. \tag{1.11}$$

where the electric permittivity $\boldsymbol{\varepsilon}$ and the magnetic permeability μ are defined as:

$$\varepsilon = \varepsilon_0 \varepsilon_i \,, \tag{1.12}$$

$$\mu = \mu_0 \mu_i \tag{1.13}$$

where ε_i is the relative permittivity of the medium, μ_i is its relative permeability of the medium. ε_0 and μ_0 are the free space permittivity and the free space permeability respectively.

Applying Eq. (1.9) to (1.13) into Eq.(1.5) to (1.8) we get:

$$\vec{\nabla} \cdot \vec{E} = 0, \tag{1.14}$$

$$\vec{\nabla} \times \vec{E} = -\mu \frac{\partial \vec{H}}{\partial t}, \tag{1.15}$$

$$\vec{\nabla} \cdot \vec{H} = 0, \tag{1.16}$$

$$\vec{\nabla} \times \vec{H} = \varepsilon \frac{\partial \vec{E}}{\partial t}. \tag{1.17}$$

1.3 The Wave Equation

Taking the curl of Eq. (1.15) to derive the wave equation

$$\vec{\nabla} \times \vec{\nabla} \times \vec{E} = -\mu \frac{\partial (\vec{\nabla} \times \vec{H})}{\partial t}, \tag{1.18}$$

Substituting Eq. (1.17) into (1.18), we get:

$$\vec{\nabla} \times \vec{\nabla} \times \vec{E} = -\mu\varepsilon \frac{\partial^2 \vec{E}}{\partial t^2}, \tag{1.19}$$

Using the vector identity

$$\vec{\nabla} \times (\vec{\nabla} \times \vec{A}) = \vec{\nabla}(\vec{\nabla}.\vec{A}) - \nabla^2 \vec{A}, \tag{1.20}$$

Substituting Eq. (1.20) into (1.19) we get:

$$\nabla^2 \vec{E} - \mu\varepsilon \frac{\partial^2 \vec{E}}{\partial t^2} = \vec{\nabla}(\vec{\nabla} \cdot \vec{E}), \tag{1.21}$$

For sources free isotropic medium $\vec{\nabla} \cdot \vec{E} = 0$, Eq. (1.21), Becomes:

$$\nabla^2 \vec{E} - \mu\varepsilon \frac{\partial^2 \vec{E}}{\partial t^2} = 0, \tag{1.22}$$

Similarly, starting with Eq. (1.17) and following the above procedure we get

$$\nabla^2 \vec{H} - \mu\varepsilon \frac{\partial^2 \vec{H}}{\partial t^2} = 0, \tag{1.23}$$

Equations (1.22) and (1.23) are three dimensional equations where the laplacian operator ∇^2 is given in rectangular coordinates by

$$\nabla^2 = \frac{\partial^2}{\partial x^2} + \frac{\partial^2}{\partial y^2} + \frac{\partial^2}{\partial z^2}, \tag{1.24}$$

Equations (1.22) and (1.23) are called Helmholtz equations which having a sinusoidal solution if the coefficient of the second term is positive and an exponentially increasing or decreasing solution if it is negative.

The ideal notation for the electromagnetic wave which represents the solution of the wave equation, is the phasor notation, i.e.

$$\psi(\vec{r},t) = \psi_0 e^{-i(k.\vec{r}-\omega t)} \tag{1.25}$$

where ψ is either E or H, ψ_0 is the amplitude of the wave, k is the wave vector and ω is the angular frequency.

Applying the phasor notation to Maxwell's equations, we get:

$$\nabla \times E = -i\,\omega\mu H, \tag{1.26}$$

$$\nabla \times H = i\,\omega\varepsilon E, \tag{1.27}$$

or

$$E = \frac{1}{i\,\omega\varepsilon}\nabla \times H, \tag{1.28}$$

$$H = -\frac{1}{i\,\omega\mu}\nabla \times E\ . \tag{1.29}$$

Eqs. (1.26) and (1.27) represent Maxwell's equations for time harmonic fields in free charge lossless media.

To analyze wave propagation in a charge-free medium, it is helpful to have separate wave equations for electric and magnetic fields.

Taking $\nabla\times$ Eq. (1.15) and substitute from Eq.(1.17) for the value of $\vec{\nabla}\times\vec{H}$, then we obtain (Born & Wolf, 1999; Markoš & Soukoulis, 2008):

. $$\vec{\nabla}\times(\vec{\nabla}\times\vec{E}) = \omega^2\mu\varepsilon E, \tag{1.30}$$

Applying Eq. (1.20) and (1.14) into (1.30) we get:

$$\nabla^2\vec{E}+\omega^2\mu\varepsilon\vec{E}=0, \tag{1.31}$$

Similarly, the homogeneous wave equation for ***H*** is:

$$\nabla^2\vec{H}+\omega^2\mu\varepsilon\vec{H}=0, \tag{1.32}$$

In a lossless medium, the wavenumber k is defined by $k^2=\omega^2\mu\varepsilon$. Then Eqn. (1.31) and Eq. (1.32) can be written as:

$$\nabla^2\vec{E}+k^2\vec{E}=0, \tag{1.33}$$

$$\nabla^2 H+k^2 H=0, \tag{1.34}$$

Eqs. (1.33) and (1.34) are referred to as Hemholtz equations.

1.4 Refractive index

The refractive index n is a measure of how speed of a wave is reduced inside the medium relative to the speed in vacuum. It is determined by the permittivity and permeability by the following relation

$$n=\sqrt{\mu_r\varepsilon_r} \tag{1.35}$$

The velocity of ray light bending when it moves from medium to another. The refraction index is also given by:

$$n=\frac{speed\ \text{of light in vecuum}}{speed\ \text{of light in a mdium}}=\frac{c}{v} \tag{1.36}$$

Where, $c=\dfrac{1}{\sqrt{\mu_0\varepsilon_0}}$ and $v=\dfrac{1}{\sqrt{\mu\varepsilon}}$

1.5 Nonlinear media

Nonlinear medium is a medium where the relative refractive index depends on intensity of light. When an external electric field is applied to a matter, it induces or reorients dipole moments of atoms or molecules of the matter, resulting in a nonzero average dipole moment per unit volume or polarization of the material. If the applied electric field is not too large, the polarization is proportional to the field strength, i.e،

$$\boldsymbol{P}=\varepsilon_0\ \chi^{(1)}\ \mathbf{E} \tag{1.37}$$

where $\chi^{(1)}$ is the usual susceptibility of linear optics. In writing Eq. (1.37) we ignored, for simplicity, the vector nature of both the applied field and the resulting polarization. As the magnitude of the field increases though, the simple linear relation Eq. (1.37) no longer holds. However, typical electric fields generated by all but most powerful modern lasers are in the range of 106 to 107 V/cm, whereas the electrons bound to atoms or molecules experience far greater fields of the order of 109 to 1010 V/cm. Consequently, one can assume the induced electron displacements in laser fields to be rather small; the latter circumstance justifies using a Taylor series expansion of the dielectric Polarization density (dipole moment per unit volume***)*** $\boldsymbol{P}(t)$ at time t in terms of the electrical field $\boldsymbol{E}(t)$:

$$\boldsymbol{P}(t) = \varepsilon_0(\chi^{(1)}\boldsymbol{E}(t) + \chi^{(2)}\boldsymbol{E}^2(t) + \chi^{(3)}\boldsymbol{E}^3(t) + \ldots), \tag{1.38}$$

The coefficients $\chi^{(n)}$ are the n-th order susceptibilities of the medium and the presence of such a term is generally referred to as an n-th order nonlinearity.

where ε_l is the real constant, α is the coefficient of nonlinearity

The propagation of light in a nonlinear medium is governed by the wave equation Eq.(1.18), which was derived from Maxwell's equations for an arbitrary homogeneous, isotropic dielectric medium. The isotropy of the medium ensures that the vectors P and E are always parallel so that they may be examined on a component-by-component basis, which provides (Iizuka, 2002)

$$\nabla\times\nabla\times E + \frac{n^2}{c^2}\frac{\partial^2}{\partial t^2}E = \frac{1}{c^2\varepsilon_0}\frac{\partial^2}{\partial t^2}P^{NL}, \tag{1.39}$$

where $\boldsymbol{P}^{NL}$ is the nonlinear part of the Polarization density and n is the refractive index due to the linear term in ***P.***

Eq.(1.39) has nonzero term at the right hand side $(\frac{\mathbf{1}}{\boldsymbol{c^2\varepsilon_0}}\frac{\boldsymbol{\partial}}{\boldsymbol{\partial t^2}}^{\mathbf{2}}\boldsymbol{P}^{NL})$ that called the inhomogeneous term and $\mathbf{P}^{\mathrm{NL}} = \varepsilon_0\chi^{(2)}\boldsymbol{E}^2$

The permittivity in kerr-meduim can ber rewritten as (Iizuka, 2002)

$$\varepsilon_{nl} = \varepsilon_l + \alpha E_z^2, \tag{1.40}$$

1.6 Boundary Conditions

The boundary conditions required for the electromagnetic fields cross a given boundary between two different media as shown in Figure (1.1) must be satisfied. A set of boundary conditions at the interface between the two media are summarized as follows (Kenji and Tsutomun, 2002):

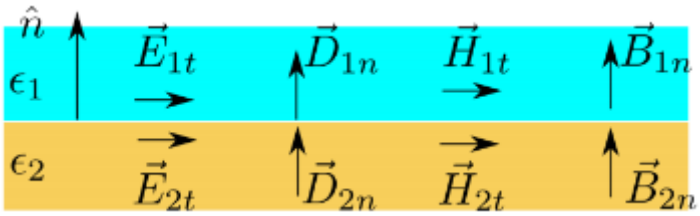

Figure (1.1): Field directions at boundary (Hunsperger, 2002).

1- The tangential component of the electric field is continuous across the surface,i.e.

$$\hat{n}_i \times (\vec{E}_{t2} - \vec{E}_{t1}) = 0,$$

$$\hat{n}_2 \times \vec{E}_{t2} = \hat{n}_1 \times \vec{E}_{t1} \qquad (1.41)$$

where $\hat{n}_i$ is the unit vector normal to the interface between the media and pointing in the outward direction relative to the region i.

2-The tangential component of the magnetic field is continuous, when no charge at the surface

$$\hat{n}_i \times (\vec{H}_{t2} - \vec{H}_{t1}) = 0,$$

$$\hat{n} \times \vec{H}_{t2} = \hat{n} \times \vec{H}_{t1} \qquad (1.42)$$

In the presence of a surface current of density $\vec{J}_s$, the tangential component of the magnetic field is discontinuous across the surface by $\vec{J}_s$, i.e.

$$\hat{n}_i \times (\vec{H}_{t2} - \vec{H}_{t1}) = \vec{J}_s, \qquad (1.43)$$

3-The normal component of the magnetic flux is continuous across the surface of discontinuity, i.e.

$$\hat{n}_i.(\vec{B}_2 - \vec{B}_1) = 0, \tag{1.44}$$

4-In the presence of a surface charge of density ρ, the normal component of the electric displacement is discontinuous by ρ, i.e.

$$\hat{n}_i.(\vec{D}_2 - \vec{D}_1) = \rho, \tag{1.45}$$

when there are no charges on the surface, the electric displacement is continuous.

$$\hat{n}_1 \cdot \vec{D}_1 = \hat{n}_2 \cdot \vec{D}_2. \tag{1.46}$$

where

$$\vec{B} = \mu\vec{H}, \tag{1.47}$$

$$\vec{D} = \varepsilon\vec{E}, \tag{1.48}$$

The importance of the boundary conditions gets clear when dealing with electromagnetic waves striking an interface between two different media.

1.7 Theory of Waveguides

1.7.1 Surface wave

The structure of the basic dielectric step index waveguide is shown in Figure (1.2). The slab waveguide consists of three layers: the film is sandwiched between cover and substrate,{which has the refractive index dielectric (n_f)}, The cover material (cladding) has refractive index (n_c), and the substrate material, has refractive index (n_s). For surface wave $n_s \succ n_f \succ n_c$. waveguide slab structure is a symmetric.

1.7.2 Guiding wave

For three layers wave guide structure, to keep the wave guide inside the film layer, the refractive index dielectric (n_f) must be larger than that of the substrate (n_s) and that of the cover (n_c) this means that $n_f \succ n_s \succ n_c$.

Moreover, the substrate and cover layers are much thicker than the operating wavelength λ. However, The film thickness d should be comparable to λ (Pollock, 1995).

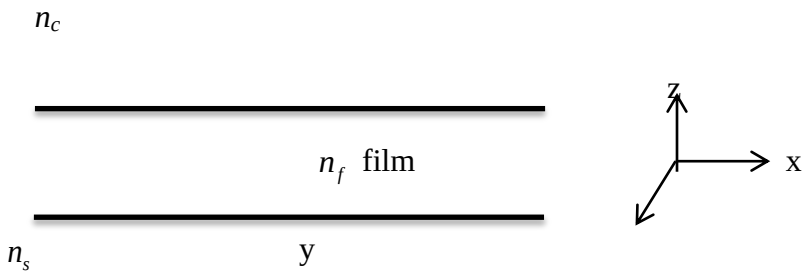

Figure (1.2): Basic dielectric step index waveguide consists of three layers

1.8 Basic Waveguide Equations

Considering an electromagnetic wave which advances into waveguide shown in Figure (1.2) and propagating in the z-direction. The electric and magnetic fields are supposed to have the sinusoidal form, as displayed in Figure (1.3).

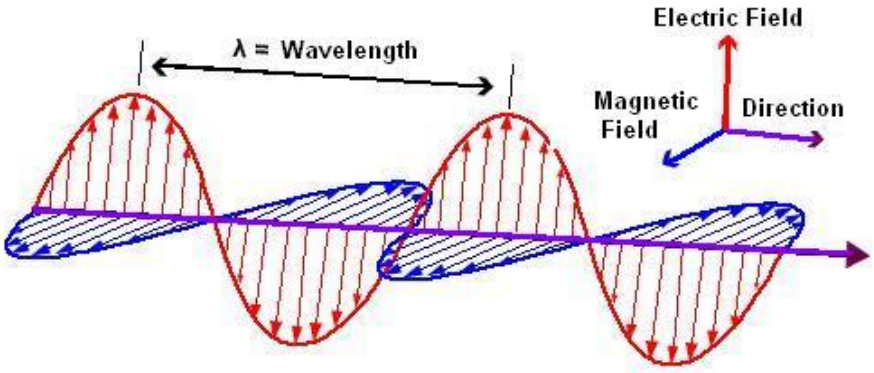

Figure (1.3): Propagation of an electromagnetic field.

The electric and magnetic field can be writen as ,

$$\vec{E} = E_0(x, y)e^{i(\omega t - \beta z)}, \tag{1.49}$$

$$\vec{H} = H_0(x, y)e^{i(\omega t - \beta z)}. \tag{1.50}$$

where ω is the frequency of the field and β is the longitudinal component of propagation in z-direction, E_0 and H_0 define the amplitude and the direction of the vectors $\boldsymbol{E}$ and $\boldsymbol{H}$, respectively.

Expanding Eq. (1.26) in three dimensions, we get:

$$\begin{vmatrix} \hat{i} & \hat{j} & \hat{k} \\ \frac{\partial}{\partial x} & \frac{\partial}{\partial y} & \frac{\partial}{\partial z} \\ E_x & E_y & E_z \end{vmatrix} = -i\,\mu\omega(H_x\hat{i} + H_y\hat{j} + H_z\hat{k}) \tag{1.51}$$

By solving Eq. (1.51) ,we get:

$$\left.\begin{aligned} \frac{\partial E_z}{\partial y} + i\,\beta E_y &= -i\,\mu\omega H_x \\ \frac{\partial E_z}{\partial x} + i\,\beta E_x &= i\,\mu\omega H_y \\ \frac{\partial E_y}{\partial x} - \frac{\partial E_x}{\partial y} &= -i\,\mu\omega H_z \end{aligned}\right\} \tag{1.52}$$

Similarly, Eq. (1.27) becomes:

$$\begin{vmatrix} \hat{i} & \hat{j} & \hat{k} \\ \frac{\partial}{\partial x} & \frac{\partial}{\partial y} & \frac{\partial}{\partial z} \\ H_x & H_y & H_z \end{vmatrix} = i\,\varepsilon\omega(E_x\hat{i} + E_y\hat{j} + E_z\hat{k}) \tag{1.53}$$

By solving Eq.(1.53) , we get:

$$\left.\begin{aligned} \frac{\partial H_z}{\partial y} + i\,\beta H_y &= i\,\varepsilon\omega E_x \\ \frac{\partial H_z}{\partial x} + i\,\beta H_x &= -i\,\varepsilon\omega E_y \\ \frac{\partial H_y}{\partial x} - \frac{\partial H_x}{\partial y} &= i\,\varepsilon\omega E_z \end{aligned}\right\} \tag{1.54}$$

1.9 Optical Waveguide Modes

The propagating modes along the waveguide can be classified according to the presence of field components in the wave. The longitudinal components are those field components that are in the direction of the wave propagation, while those perpendicular to the direction of propagation are defined as transverse components (Blake, 1969; Pozar, 2009).

1.9.1 General Solutions for Optical Waveguide Modes

The analysis of planar waveguide requires solving Helmholtz equation in the three layers. Consider again the waveguide shown in Figure (1.2). The wave is supposed to propagate in the z-direction. The waveguide is assumed to be infinitely extended in the y-direction, so that $\frac{\partial}{\partial y} = 0$ (Chen, 2006).

Then Eqs. (1.53) and (1.54) become:

$$i\,\beta E_y = -i\,\mu_0\omega H_x, \tag{1.55}$$

$$\frac{\partial E_z}{\partial x} + i\,\beta E_x = i\,\mu_0\omega H_y, \tag{1.56}$$

$$\frac{\partial E_y}{\partial x} = -i\,\mu_0\omega H_z, \tag{1.57}$$

$$i\,\beta H_y = i\,\varepsilon\omega E_x, \tag{1.58}$$

$$\frac{\partial H_z}{\partial x} + i\,\beta E_x = -i\,\varepsilon\omega E_y, \tag{1.59}$$

$$\frac{\partial H_y}{\partial x} = i\,\varepsilon\omega E_z\,. \tag{1.60}$$

The ratio of the propagation constant in the medium β to the wave number in a vacuum k_0 is called the effective index:

$$N = \frac{\beta}{k_0}. \tag{1.61}$$

Therefore , the Helmholtz equation for the electric field $\vec{E}$ in Eq. (1.33) can be rewritten as:

$$\nabla^2\vec{E} + (k_i^2 - \beta^2)\vec{E} = 0, \tag{1.62}$$

or

$$\nabla^2 E + \gamma_i^2 E = 0, \tag{1.63}$$

Similarity the Helmholtz equation for the Magnetic field $\vec{H}$ in Eq. (1.34) can be rewritten as:

$$\nabla^2 H + (k_i^2 - \beta^2)H = 0, \tag{1.64}$$

or

$$\nabla^2 H + \gamma_i^2 H = 0. \tag{1.65}$$

where

$$k_i^2 - \beta^2 = \gamma_i^2 \tag{1.66}$$

with γ_i^2 is transvers wave number, $k_i = \sqrt{\varepsilon_i \mu_i}\,k_0$, i=1,2,3 is the wavenumber in region i, $k_0 = \omega\sqrt{\varepsilon_0\mu_0} = \omega/c$ is the free-space wavenumber, and $\varepsilon = \varepsilon_0\varepsilon_i, \mu = \mu_0\mu_i$, where ε_i and μ_i are the relative permittivity and permeability of the region i.

1.9.2 Transverse electric mode (TE mode).

In the TE mode, the electric field has no longitudinal component (E_z=0) but in the transverse direction ($E_y \neq 0$). Only three components exist for TE mode E_y , H_x and

H_z. The two magnetic field components H_x and H_z can be expressed in terms of the electric field component E_y by using Eq.(1.52) (Kenji & Tsutomu, 2001):

$$H_x(x) = -\frac{\beta}{\omega\mu} E_y(x), \tag{1.67}$$

$$H_z(x) = \frac{i}{\omega\mu} \frac{d}{dx} E_y(x) \tag{1.68}$$

Substituting from Eqs. (1.67) and (1.68) into Eq. (1.59) gives the Helmholtz wave equation for TE mode:

$$\frac{d^2}{dx^2} E_y(x) + (k_i^2 - \beta^2) E_y(x) = 0 \tag{1.69}$$

1.9.3 Transverse Magnetic (TM) modes:

The magnetic field is transverse to the direction of propagation (no longitudinal magnetic field component) while the electric field has both transverse and longitudinal component [$H_z = 0$, $E_z \neq 0$].

1.9.4 Transverse Electromagnetic (TEM) modes:

The transverse electric and magnetic (TEM) modes are perpendicular to the direction of wave propagation with no longitudinal components [$E_z = H_z = 0$]. TEM modes cannot exist on single conductor guiding structures. Plane waves can also be classified as TEM modes. **Quasi-TEM Modes** – modes which approximate true TEM modes when the frequency is sufficiently small.

$$\lim_{f \to 0} E_z = \lim_{f \to 0} H_z = 0 \tag{1.70}$$

1.9.5 Hybrid Modes (EH or HE modes):

Both the electric and magnetic fields have longitudinal components [$E_z \neq H_z \neq 0$]. The longitudinal electric filed is dominant in the EH mode while the longitudinal magnetic field is dominant in the HE mode.

Chapter 2
Graphene Material and Optical Sensing

Chapter 2
Graphene Material and Optical Sensing

This chapter presented some facts about Graphene such as its definition, characteristics, brief history, Optical conductivity and its applications. It also introduces the optical sensing including their concepts and their applications.

2.1 Graphene Material

Introduction

The element carbon is an unusual element. Its quasi-2-dimensional structures have attracted physicists around the globe. Real 2-dimensional states of matter have been assumed not to exist (Zhang, et al,2005).

It is stronger than diamond, conducts electricity and heat better than any material ever discovered, and has interesting optical response. Also, its reflectance, transmittance and absorbance are one of the striking optical properties of Graphene (Nair et al., 2008; Kuzmenko et al, 2008). Graphene is the thinnest ever material known in the world. Thus , so for this feature it plays major rules in the fundamental base for technology development, which included technological industry such as electronic optical.

The previous attempts to study graphene can be traced back to 1859. There has been an explosion in research around the material since 2004, when Professor Sir Andre Geim and Professor Sir Kostya Novoselov of the University of Manchester discovered and isolated a single atomic layer of carbon for the first time. The pair received the Nobel Prize in Physics in 2010 in recognition of their breakthrough(Nikitin, 2011).

2.2 Brief History

Graphene, millions of ultra-thin layers that stack together to form graphite commonly found in pencils, was first studied as long ago as 1947.Graphene was first studied theoretically in the 1940s. At that time, scientists thought it was physically impossible for a two dimensional material to exist, so they did not pursue isolating graphene. Decades later, interest picked up and researchers began dreaming up

techniques to peel apart graphite. They tried wedging molecules between layers of graphene and scraping and rubbing graphite, but they never got to a single layer. Eventually, they were able to isolate graphene on top of other materials, but not on its own.

Attempts to grow graphene on other single crystal surfaces have been ongoing since the 1970s, but strong interactions with the surface on which it was grown always prevented the true properties of graphene being measured experimentally

The electric current would be carried by effectively massless charge carriers in graphene was pointed out theoretically in 1984, and the name 'graphene' was first mentioned in 1987 to describe the graphite layers that had various compounds inserted between them. The term was used extensively in work on carbon nanotubes, which are rolled up graphene sheets.

In 2002, University of Manchester researcher Andre Geim became interested in graphene and challenged a PhD student to polish a hunk of graphite to as few layers as possible. The student was able to reach 1,000 layers, but could not hit Geim's goal of 10 to 100 layers. Geim tried a different approach: tape. He applied it to graphite and peeled it away to create flakes of layered graphene. More tape peels created thinner and thinner layers, until he had a piece of graphene 10 layers thick.

While scientists had theorized about graphene for decades, it was first produced in the lab in 2004. Despite its short history, graphene has already revealed a cornucopia of new physics and potential applications. Andre Geim and Konstantin Nevoselov at the university of Manchester won the Nobel prize in physics in 2010 "for groundbreaking experiments regarding the two-dimensional material graphene" (Xia et al, 2009).

2.3 Definition of Graphene

Graphene is, basically, a single atomic layer of graphite; an abundant mineral which is an allotrope of carbon that is made up of very tightly bonded carbon atoms organized into a hexagonal lattice.

2.4 Structure of graphene

Sheets of graphene are bonded by loose bond in graphite, these bonds are broken and sheets are isolated to form graphene. These isolated hexagonal sheets are graphene .

It is the one-atom thick planar sheet of carbon atoms (graphite), which makes it the thinnest material ever discovered and has 2-dimentional crystalline allotrope of carbon. It is almost completely transparent, yet so dense that not even helium can pass through it(Morozov, et al., 2004).

2.5 Prepare

The isolation of single graphene sheets offers opportunities for its investigation by various spectroscopic and microscopic techniques. Samples can be either in the form of dispersion or graphene sheets deposited on the proper substrates. In this section the most commonly used characterization tools are introduced. As for most nanomaterials electronic microscopies and AFM are powerful tools for the characterization of graphene and graphene derivatives. Raman spectroscopy and spectromicroscopy can distinguish single layer graphene from double layer and few-layer graphene and give clear indications on the number of defects present in the material. Thermogravimetric analysis (TGA) diagrams are useful to trace changes in the structure of graphitic materials before and after functionalization of graphene sheets. Optical microscopy can visualize a single graphene layer that is placed on the right substrate. X-ray diffraction (XRD) informs on the success of exfoliation or intercalation of graphite and is particularly useful to demonstrate functionalization.(Xu, et al., 2012).

2.6 Propriety

Geim and Novoselov's paper was wildly interesting to other scientists because of its description of graphene's strange physical properties. Electrons move through graphene incredibly fast and begin to exhibit behaviors as if they were massless, mimicking the physics that governs particles at super small scales.

2.6.1 ConductiveThermal

A graphene sheet is thermodynamically most stable

1. Only for molecules larger than 24,000 atoms

2. Size greater than 20 nm

3.Thermal conductivity is measured to be between $(4.84\pm0.44) \times 10^3$ and $(5.30\pm0.48) \times 10^3$ $W \cdot m-1 \cdot K-1$

2.6.2 Electronic Properties

One of the most useful properties of graphene is that it is a zero-overlap semimet al (with both holes and electrons as charge carriers) with very high electrical conductivity. Carbon atoms have a total of 6 electrons; 2 in the inner shell and 4 in the outer shell. The 4 outer shell electrons in an individual carbon atom are available for chemical bonding, but in graphene, each atom is connected to 3 other carbon atoms on the two dimensional plane, leaving 1 electron freely available in the third dimension for electronic conduction. These highly-mobile electrons are called pi (π) electrons and are located above and below the graphene sheet. These pi orbitals overlap and help to enhance the carbon to carbon bonds in graphene. Fundamentally, the electronic properties of graphene are dictated by the bonding and anti-bonding (the valance and conduction bands) of these pi orbitals(Morozov et al., 2004).

2.6.3 Mechanical

The carbon–carbon bond length in graphene is about 0.142 nanometers. Graphene sheets stack to form graphite with an interplanar spacing of 0.335 nm.Graphene is the strongest material ever tested, with an intrinsic tensile strength of 130 GPa and a Young's modulus (stiffness) of 1 TPa (150000000 psi). The Nobel announcement illustrated this by saying that a 1 square meter graphene hammock would support a 4 kg cat but would weigh only as much as one of the cat's whiskers, at 0.77 mg (about 0.001% of the weight of 1 m^2 of paper). The spring constant of suspended graphene sheets has been measured using an atomic force microscope (AFM). Graphene sheets were suspended over SiO_2 cavities where an AFM tip was used to apply a stress to the sheet to test its mechanical properties. Its spring constant was in the range 1–5 N/m and the stiffness was 0.5 TPa, which

differs from that of bulk graphite. These intrinsic properties could lead to applications such as pressure sensors and resonators.

Due to its large surface energy and out of plane ductility, flat graphene sheets are unstable with respect to scrolling, i.e. bending into a cylindrical shape, which is its lower-energy state(Neto, et al,. 2009).

2.6.4 Optical Conductivity of Graphene

The dynamic optical conductivity of graphene can be determined from the Kubo formalisms (Hanson, 2008 et al.,Gusynin 2006), consisting of intra-band and inter-band contributions;

$$\sigma(\omega,\mu_c,\tau,T)=\frac{ie^2(\omega-i\tau^{-1})}{\pi\hbar^2}\left[\frac{1}{(\omega-i\tau^{-1})}\int_0^\infty \xi\left(\frac{\partial f_d(\xi)}{\partial\xi}-\frac{\partial f_d(-\xi)}{\partial\xi}\right)d\xi-\int_0^\infty\frac{\partial f_d(-\xi)-\partial f_d(\xi)}{(\omega-i\tau^{-1})-4(\xi/\hbar)^2}d\xi\right]. \quad (2.1)$$

where e is the charge of an electron, ξ is the energy, $\hbar$ is the reduced Planck's constant, $f_d(\xi)=(e^{(\xi-\mu_c)/k_BT}+1)^{-1}$ is the Fermi-Dirac distribution, ω is the radian frequency, k_B is the Boltzmann's constant, T is the temperature, μ_c is the chemical potential, which can be varied by doping and/or an applied bias, τ is the relaxation time (τ^{-1} is the scattering rate), i is the imaginary unit and $e^{\,i\omega t}$ is the time variation. The first part in Eq. (2.1) is due to the intraband contribution and the second is due to interband contribution. The intra-band contribution can be derived and simplified as,

$$\sigma_{intra}(\omega)=-i\,\frac{e^2k_BT}{\pi\hbar^2(\omega-i\tau^{-1})}\left[\frac{\mu_c}{k_BT}+2\ln(e^{(-\mu_c)/k_BT}+1)\right]. \quad (2.2)$$

While the inter-band can be approximated as, for $k_BT<<|\mu_c|,\hbar\omega$:

$$\sigma_{intea}(\omega)=\frac{-ie^2}{4\pi\hbar}\ln\left(\frac{2|\mu_c|-(\omega-i\tau^{-1})\hbar}{2|\mu_c|+(\omega-i\tau^{-1})\hbar}\right). \quad (2.3)$$

The conductivity of Graphene is normalized by σ_0 (Xu et al., 2012).

where $$\sigma_0=\frac{\pi e^2}{2h}=6.085\times10^{-5}simens\ .$$

2.7 Application of Graphene

Graphene amazing properties brings scope of various future applications in following Fields.Graphene is a disruptive technology; one that could open up new markets and even replace existing technologies or materials. It is when graphene is used both as an improvement to an existing material and in a transformational capacity that its true potential could be realised.Graphene detects. Ultra-sensitive sensors made from graphene could detect minute dangerous particles helping to protect potentially dangerous environments (Zhang, et al, 2005).

2.7.1 Graphene sensors

Graphene is an ideal material for sensors. Graphene and sensors are a natural combination, as graphene's large surface-to-volume ratio, unique optical properties, excellent electrical conductivity, high carrier mobility and density, high thermal conductivity and many other attributes can be greatly beneficial for sensor functions.

Graphene is thought to become especially widespread in biosensors and diagnostics. Graphene will enable sensors that are smaller and lighter - providing endless design possibilities. They will also be more sensitive and able to detect smaller changes in matter, work more quickly and eventually even be less expensive than traditional sensors. Some graphene-based sensor designs contain a Field Effect Transistor (FET) with a graphene channel. Upon detection of the targeted analyte's binding, the current through the transistor changes, which sends a signal that can be analyzed to determine several variables.

Graphene-based nanoelectronic devices have also been researched for use in DNA sensors (for detecting nucleobases and nucleotides), Gas sensors (for detection of different gases), PH sensors, environmental contamination sensors, strain and pressure sensors, and more (Xu et al, 2012).

2.7.2 Graphene electronics

Graphene can be used as a coating to improve current touch screens for phones and tablets. It can also be used to make the circuitry for our computers making them incredibly fast. These are just two examples of how graphene can enhance today's devices. Graphene can also spark the next-generation of electronics (Xia et al, 2009).

2.7.3 Graphene Transistors

Researchers at the University of Manchester have already created the world's smallest transistor using graphene. The smaller the size of the transistor, the better they perform within circuits. The fundamental challenge facing the electronics industry in the next 20 years is the further miniaturisation of technology (Xu, et al, 2012).

2.7.4 Graphene Semiconductors

Graphene's unique properties of thinness and conductivity have led to global research into its applications as a semiconductor. At just one atom thick and with the ability to conduct electricity at room temperature graphene semiconductors could replace existing technology for computer chips. Research has already shown that graphene chips are much faster than existing ones made from silicon (Wang et al, 2008).

2.8 Optical Waveguide Sensors

Waveguide sensors consider as one of the most important applications of planar waveguides. Sensing is performed by the evanescent field in the covering medium (Parriaux and Dierauer, 1994). The effective refractive index of a waveguide structure depends on film thickness and refractive indices of both film and surroundings. Thus, if the biological or chemical changes result in changing the effective refractive index, then the new properties give information about the refractive index of the analyte or the thickness of the adsorbed layer. Sensing process is then the measure of change in effective index due to either changes in cover refractive index or adding an ultra-thin film on surface of the guiding film.

The sensitivity of the measurement of physical or chemical quantity present in the cover depends on the strength and the distribution of the evanescent field in the cover. The main design task is therefore to find the waveguide structure which maximizes the sensitivity on the quantity to be measured. The analysis differs somewhat if the measured property is homogeneously distributed in the cover or it is an ultra thin film at the waveguide–cover interface (surface sensing). The two cases are illustrated schematically in Figure (2.1) and Figure (2.2). It is assumed hereafter that the cover medium is a liquid or a gas, which implies that the contact zone

between the cover and the waveguide surface is of zero thickness and does not exhibit an air film or bubbles.

2.8.1 Homogeneous sensing

If the properties are homogeneously distributed in the waveguide cover, then the process of detecting changes of these properties is called homogeneous sensing. Here sensitivity is defined as the change in the effective refractive index through the cover medium,

$$S_{d_A} = \frac{\partial N}{\partial d_A}, \qquad S_{n_A} = \frac{\partial N}{\partial n_A}.$$

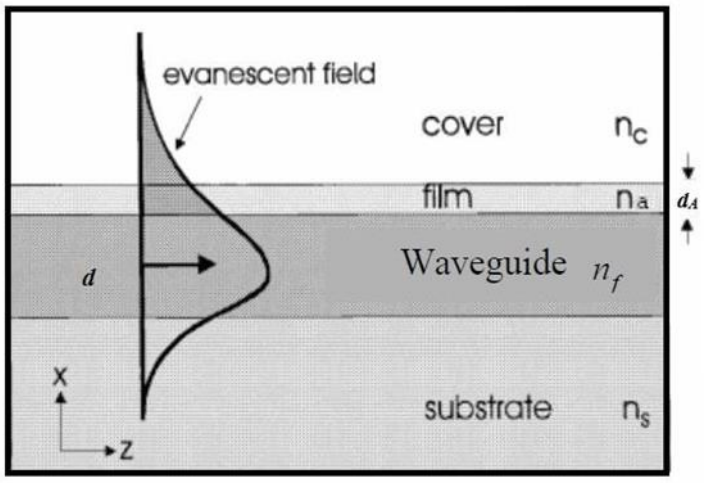

Figure (2.1): Schematic representation of planar waveguide homogeneous sensor (Parriaux & Veldhuis, 1998).

2.8.2 Surface sensing

If changes of optical properties are due to adsorption of some molecules that construct an ultra-thin film on surface of the guiding thin film, then the process of detecting the adsorbed molecules is said to be surface sensing.

In such configurations, the sensor consists of a guiding film over which sets a sensing layer. Electromagnetic waves propagating along the sensing element are attenuated due to the additional adsorbed film or analyte concentration.

Mathematically, surface sensing is defined as the change of effective refractive index with respect to change in adlayer width(Parriaux and Velduis,1998)

$$S_{n_c} = \frac{\partial N}{\partial n_c}. \qquad (2.4)$$

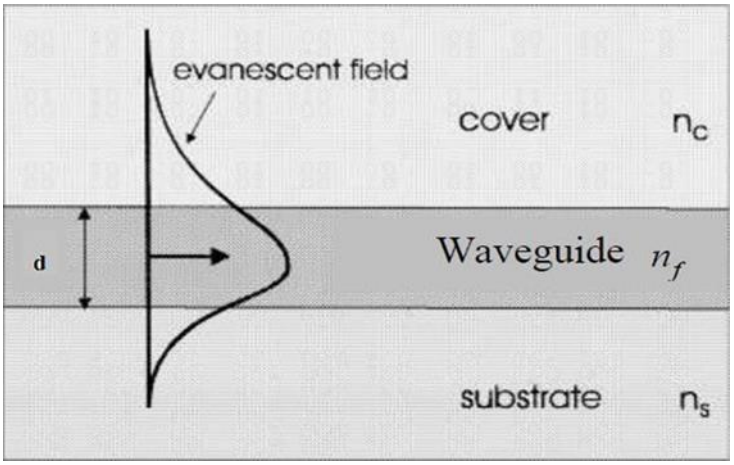

Figure (2.2): Schematic representation of planar waveguide surface sensor (Parriaux & Veldhuis, 1998).

2.8.3 Uses and applications

Planar optical waveguide sensors are used in many aspects: detecting and measuring the thickness of any layers such as metals, metal compounds, organic, bio-organic, enzymes, antibodies and microbes. They are also used in measuring concentrations of liquids and detecting small traces in chemicals.

One of the important uses of such sensors is in radiation dosimeters and protective masks or clothing when they can readily identify and give scanning data about any change in exposure or lack in protection. They are of great benefit in detecting drug vapors. More specifically, planar optical sensors are also used in any chemical, biological or physical processes accompanied with changes in strength and distribution of the evanescent field strength (Xu et al, 2012).

2.9 Previous Work

A lot of researches and experiment studies have been conducted to improve the sensitivity of waveguide sensors. Sensing the evanescent field has captured considerable attention due to their advantages.Now well it has been proven and has been developed sensor systems and clear from many of the investigators. Studies have focused on the sensor board to promote the resolution, in and out of the whole system, reduce cost, and maximize the sensitivity of the sensor basis. Therefore , several structures by selecting the appropriates layer have been proposed to enhance sensor sensitivity. For example, the addition of metamaterials to the sensor structure have been investigated by many authors (El-Khozondar et al., 2015a; 2015b; 2014; 2012a; 2012b; 2012e; 2011; 2008a; 2008b; 2008; 2006)

Shabat et al., (2007) proposed optical waveguide sensors in which one or both of the surrounding media have an intensity dependent refractive index El-Khozondar, Rifa El-Khozondar et al., 2007 have studied the influence of temperature stress of the thermal sensitivity effective refractive index for asymmetrical nonlinear optical waveguides. It is found that the thermal sensitivity of the sensor can be controlled by temperature stresses which can be controlled by carefully picking the materials and loading methods. Wang et al.(2008) have studied the coupling surface plasmons in monolayer graphene sheet array and proved that the coupling of surface plasmons in the individual graphene sheet results in a reduction of the modal wavelength of the surface plasmons in comparison with that of a single graphene sheet The optical coupling of Plasmon waves between two graphene sheets sandwiched in symmetric surrounding dielectrics has been investigated for graphene-based high-speed and ultra-compact optoelectric devices (Wang, et al., 2012). Recently, Hamada et al.(2015) have studied the Plasmon characteristics in multilayer graphene film sandwiched by anisotropic dielectric and water cover. It is found that sensitivity of the multilayer structure containing graphene have a higher values by tuning some physical parameters as graphene thickness and the operating frequency.

Chapter 3

Three-Layers Planar Waveguide Sensor Containing Graphene (TE-Mode)

Chapter Three

Three-Layers Planar Waveguide Sensor Containing Graphene (TE-Mode)

In this chapter, three-layer slab waveguide structure is considered for sensing applications. Surface charge is assumed to be at the graphene interface. We concentrate on TE-polarized light only in this calculation. The dispersion relation is derived and the sensitivity is calculated, analyzed and discussed.

3.1 Structure Analysis

In this section, the proposed structure consists of three layers where graphene thin layer is sandwiched between dielectric medium with permittivity ε_2 and air with permittivity ε_3 and nonlinear substrate. The permittivity function of the nonlinear substrate depends on the intensity of the light and it is written as:

$$\varepsilon_1 = \varepsilon_l + \alpha E_y^2, \tag{3.1}$$

The thickness of a thin layer graphene is t_g = 0.35 nm between the dielectric layer and the air cladding. The t_g value can be considered too small so $t_g \rightarrow 0$ limit.

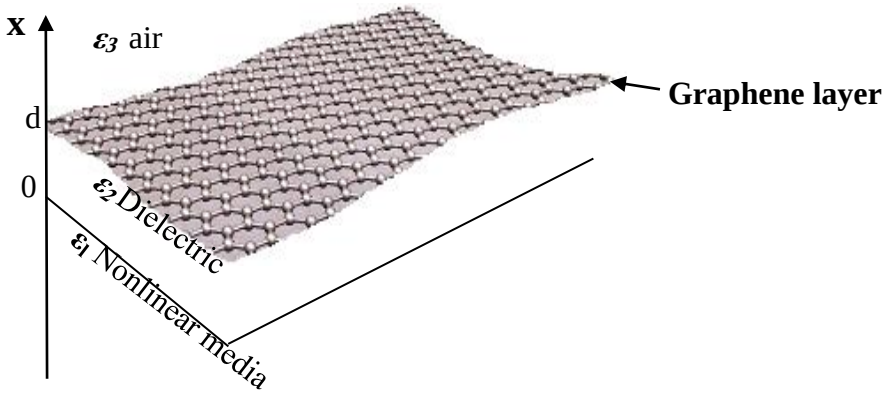

Figure (3.1): A schematic of a three-layer slab waveguide sensor including graphene material.

It can be assumed the thickness of the conducting graphene layer is infinitesimally thin with constant conductivity σ .

The proposed waveguide sensor has been investigated to find the sensitivity which can be tuned by changing variables such as the waveguide thickness and other physical parameters.

3.2 **Dispersion Equations:**

The electromagnetic responses of grapheme dielectric are numerically simulated .based on the model in Figure.3.1 the wave propagates in the Z-direction. In classical electromagnetic description, the TE wave is perpendicular to the plane of incidence (*xz*), and guiding surfaces are parallel to the *yx* plane possesses the electromagnetic field components $E = \{0, E_y, 0\}$, and $H = \{ H_x, 0 , H_z \}$.

As in chapter 1, the wave propagates in the Z-direction which has the following from:

$$\vec{E}(\vec{r},t) = \vec{E}_0(x)e^{i(\omega t-\beta z)}, \tag{3.2}$$

$$\vec{H}(\vec{r},t) = \vec{H}_0(x)e^{i(\omega t-\beta z)}, \tag{3.3}$$

Rewriting Maxwell's equations in three dimensions,

$$\begin{vmatrix} \hat{i} & \hat{j} & \hat{k} \\ \frac{\partial}{\partial x} & \frac{\partial}{\partial y} & \frac{\partial}{\partial z} \\ 0 & E_y & 0 \end{vmatrix} = -i\,\mu_0\mu_i\,\omega(H_x\hat{i} + 0\hat{j} + H_z\hat{k}), \tag{3.4}$$

and

$$\begin{vmatrix} \hat{i} & \hat{j} & \hat{k} \\ \frac{\partial}{\partial x} & \frac{\partial}{\partial y} & \frac{\partial}{\partial z} \\ H_x & 0 & H_z \end{vmatrix} = i\varepsilon_0\varepsilon_i\omega(0\hat{i} + E_y\hat{j} + 0\hat{k}) + \sigma E_y, \tag{3.5}$$

From Eqn. (3.2), (where $\frac{\partial}{\partial z} = -i\beta$) and using Eq. (3.4) we get:

$$H_x(x) = -\frac{\beta}{\omega\mu_0\mu_i} E_y(x), \tag{3.6}$$

$$H_z(x) = -\frac{1}{i\omega\mu_0\mu_i}\frac{d}{dx} E_y(x), \tag{3.7}$$

where, $\mu_0 = \mu_2 = \mu_3 = 1$

The y-component of Eq. (3.5) is given by

$$-i\beta H_x - \frac{\partial H_z}{\partial x} = \varepsilon\varepsilon_i i\omega E_y + \sigma E_y \tag{3.8}$$

For a linear medium (dielectric (2), air (3)) using Eq. (1.62), we have

$$\frac{\partial^2}{\partial x^2} E_y(x) + k_0^2(\varepsilon_i\mu_i - N^2)E_y(x) = 0; \qquad (i = 2,3). \tag{3.9}$$

where $N^2 = \frac{\beta^2}{k_0^2}$ is the effective wave index of the waveguide, $k_0 = \omega\sqrt{\mu_0\varepsilon_0}$, is the wave number in vacuum.

The filed equation for nonlinear medium (1) is similar to Eq.(3.9):

$$\frac{\partial^2}{\partial x^2} E_y(x) + k_0^2(\varepsilon_i\mu_i - N^2)E_y(x) + \alpha k_0^2 \left|E_y\right|^3 = 0; \qquad (i = 1). \tag{3.10}$$

where,

$$\gamma_1 = k_0\sqrt{N^2 - \varepsilon_1} \tag{3.11}$$

Both sides of Eq. (3.10) are first multiplied by 2 $\frac{dE_y(x)}{dx}$ and then integrated with respect to x. The result is

$$\left(\frac{dE_y(x)}{dx}\right)^2 - \gamma_1^2 E_y^2(x) + \frac{1}{2}\alpha k^2 E_y^4(x) = \Lambda \tag{3.12}$$

Let us determine the integration constant Λ. Since Eq. (3.12) has to hold regardless of the value of x, the location of the boundary condition is chosen to be at the location of the peak. The condition is

$$\frac{dE_y(x_0)}{dx} = 0, \tag{3.13}$$

Setting Λ=0 in Eq.(3.12), we get the of E_y to be,

$$E_y{}^2(x_0) = \frac{\gamma_1^2}{(\frac{1}{2}\alpha k_0{}^2)} \tag{3.14}$$

Let the desired type of solution $E_y(x)$ have a peak value of $\frac{\gamma_1^2}{(\frac{1}{2}\alpha k_0{}^2)}$ at the extremum. At such a location, Eq.(3.12) becomes

$$\Lambda = \frac{\gamma_1^2}{(\frac{1}{2}\alpha k^2)}(-\gamma_1^2 + \gamma_1^2) = 0 \tag{3.15}$$

$$\left(\frac{dE_y(x)}{dx}\right)^2 - \gamma^2{}_1 E_y^2(x) + \frac{1}{2}\alpha k^2 E_y^4(x) = 0 \tag{3.16}$$

Now, using the following integral from a table of integrals,

$$\int dx = \frac{1}{\sqrt{(\frac{1}{2}\alpha k^2)}} \int \frac{dE}{E\sqrt{\frac{\gamma_1^2}{(\frac{1}{2}\alpha k^2)} - E^2}} \tag{3.17}$$

$$\int \frac{dx}{x\sqrt{a^2 - x^2}} = \frac{1}{a}\sec h^{-1}\left|\frac{x}{a}\right|^2 \tag{3.18}$$

the integral of Eq. (3.20) becomes

$$x - x_0 = \frac{1}{\gamma_1}\sec h^{-1}\left(\frac{\sqrt{(\frac{1}{2}\alpha k^2)}}{\gamma_1} E_y(x)\right) \tag{3.19}$$

Thus, the final result is

$$E_y(x) = \frac{\gamma_1}{\sqrt{(\frac{1}{2}\alpha k^2)}} \sec h(\gamma_1(x - x_0)) \tag{3.20}$$

x_0 is a constant of integration at which power is maximum

Eq. (3.9) and Eq. (3.10) can be solved to obtain cladding and film fields as follows:

$$E_y(x) = \begin{cases} A\, e^{-\gamma_3 x} & x > d \\ \mathrm{B}\ \sin(\gamma_2 x) + C\cos(\gamma_2 x) \quad \text{(guided wave)} & 0 \le x \le d \\ \sqrt{\frac{2}{\alpha}}\ \frac{\gamma_1}{k_0}\ \mathrm{sech}(\gamma_1 (x - x_0)) & x < 0 \end{cases} \tag{3.21}$$

Where A, B and C are constants giving the wave amplitudes in the four layers. They can be determined from the boundary conditions. The parameters $\gamma_2 and\, \gamma_3$ are given by the forms:

$$\gamma_2 = k_0 \sqrt{\varepsilon_2 - N^2} \tag{3.22}$$

and

$$\gamma_3 = k_0 \sqrt{N^2 - n_3^2} \tag{3.23}$$

The H_z in the three layers of the waveguide structure is obtained by substituting Eq. (3.21) into Eq.(3.7) and given by

$$H_z(x) = \begin{cases} \frac{\gamma_3}{\mu\, i\omega} A\, e^{-\gamma_3 x} & x > d \\ -\frac{\gamma_2}{\mu\, i\omega}\left(\mathrm{B}\cos(\gamma_2 x)\right) - C\ \sin(\gamma_2 x)\ ) \quad \text{(guided wave)} & 0 \le x \le d \\ \frac{\gamma_1}{\mu\, i\omega}\sqrt{\frac{2}{\alpha}}\ \frac{\gamma_1}{k_0}\ \mathrm{sech}(\gamma_1 (X - X_0))\tanh(\gamma_1 (x - x_0)) & x < 0 \end{cases} \tag{3.24}$$

Applying the boundary conditions:

1) At $x = 0$

$$E_y^{(1)} = E_y^{(2)} \tag{3.25}$$

when substituting in Eq.(3.24) we get:

$$C = \sqrt{\frac{2}{\alpha}}\frac{\gamma_1}{\kappa_0}\sec h(\gamma_1 x_0) \tag{3.26}$$

when substituting in Eq.(3.21). we get:

$$H_z^{(1)} - H_z^{(2)} = 0 \tag{3.27}$$

$$\frac{\gamma_2}{\mu\, i\omega} B = \frac{\gamma_1}{\mu\, i\omega}\sqrt{\frac{2}{\alpha}}\frac{\gamma_1}{\boldsymbol{k}_0}\ \mathrm{sech}(\gamma_1(-X_0))\tanh(\gamma_1(-x_0)) \tag{3.28}$$

2) At $x = d$

$$E_y^{(3)} = E_y^{(2)} \tag{3.29}$$

when substituting in Eq.(3.21) we get:

$$A\, e^{-\gamma_3 d} = \sqrt{\frac{2}{\alpha}}\frac{\gamma_1}{k_0}\ \mathrm{sech}(\gamma_1 x_0)\{\cos(\gamma_2 d) + \frac{\gamma_1}{\gamma_2}\tanh(\gamma_1 x_0)\sin(\gamma_2 d)\} \tag{3.30}$$

$$H_z^{(3)} - H_z^{(2)} = \sigma E_y^{(3)} \tag{3.31}$$

when substituting in Eq.(3.15) we get:

$$-\frac{\gamma_3}{\mu\, i\omega} A\, e^{-\gamma_3 d} - \frac{\gamma_2}{\mu\, i\omega}\sqrt{\frac{2}{\alpha}}\,\frac{\gamma_1}{\kappa_0}\,\mathrm{sech}(\gamma_1 x_0)\,\{-\frac{\gamma_1}{\gamma_2}\tanh(\gamma_1 x_0)\,\cos(\gamma_2 d) - \sin(\gamma_2 d)\} = \sigma\, A\, e^{-\gamma_3 d} \quad (3.32)$$

3.3 Approximation Solution

The dispersion equation can be written as:

$$\left(\sigma + \frac{\gamma_3}{\mu\, i\omega}\right) - \frac{\gamma_2}{\mu\, i\omega}\frac{\gamma_1}{\gamma_2}\tanh(\gamma_1 x_0) = \left(-\frac{\gamma_1}{\gamma_2}\left(\sigma + \frac{\gamma_3}{\mu\, i\omega}\right)\tanh(\gamma_1 x_0) - \frac{\gamma_2}{\mu\, i\omega}\right)\tan(\gamma_2 d) \quad (3.33)$$

$$\tan(\gamma_2 \mathrm{d} - \mathrm{m}\pi) = \frac{\left(\frac{-\gamma_2}{(\mathrm{i}\sigma\omega - \gamma_3)} - \frac{\gamma_2}{\gamma_1 \tanh(\gamma_1 x_0)}\right)}{\left(1 - \frac{\gamma_2}{(\mathrm{i}\sigma\omega - \gamma_3)}\frac{\gamma_2}{\gamma_1 \tanh(\gamma_1 x_0)}\right)} \quad (3.34)$$

$$\tan(\gamma_2 \mathrm{d} - \mathrm{m}\pi) = \frac{(\mathrm{u} + \mathrm{v})}{(1 - \mathrm{uv})} \quad (3.35)$$

where,

$$\mathrm{u} = \frac{-\gamma_2}{(\mathrm{i}\sigma\omega - \gamma_3)} \quad (3.36)$$

and

$$\mathrm{v} = -\frac{\gamma_2}{\gamma_1 \tanh(\gamma_1 x_0)} \quad (3.37)$$

$$\mathrm{v} = -\frac{\gamma_2}{\gamma_1\sqrt{1 - \frac{\alpha k_0^2 \mathrm{E}_y^2}{2\gamma_1^2}}} \quad (3.38)$$

The Eq. (3.35) can be rewritten as:

$$R_1 - R_2 = 0 \quad (3.39)$$

where,

$$R_1 = \tan(\gamma_2 d - m\pi) \tag{3.40}$$

$$R_2 = (\frac{u + v}{1 - uv}) \tag{3.41}$$

3.4 Sensitivity

The sensitivity of the evanescent field sensor Eq.(2.4) is obtained from the dispersion relation.

To find a mathematical expression for *S*, we differeniate the dispersion Eq. (2.4) with respect to n_3 as:

$$\frac{\partial R_1}{\partial n_3} - \frac{\partial R_2}{\partial n_3} = 0 \tag{3.42}$$

Differentiating Eq. (3.40) with respect to n_3 become:

$$\frac{\partial R_1}{\partial n_3} = -\frac{\sec^2(\gamma_2 d - m\pi) d \; k_0^2 N \; S}{\gamma_2} = ZS \tag{3.43}$$

where,

$$Z = -\frac{\sec^2(\gamma_2 d - m\pi) d \; k_0^2 N}{\gamma_2} \tag{3.44}$$

Differentiating Eqn. (3.41) with respect to n_3 become:

$$\frac{\partial R_2}{\partial n_3} = \frac{(u' + v')(1 - uv) - (u + v)(-u'v - uv')}{(1 - uv)^2} \tag{3.45}$$

Differentiating Eqn.(3.36)

$$\frac{\partial u}{\partial n_3} = \frac{-\gamma`_2(j\sigma\omega - \gamma_3) - \gamma_2 \gamma`_3}{(j\sigma\omega - \gamma_3)^2} \tag{3.46}$$

where,

$$\frac{\partial \gamma_1}{\partial n_3} = \frac{k_0^2 N S}{\gamma_1} \tag{3.47}$$

$$\frac{\partial \gamma_2}{\partial n_3} = \frac{-k_0^2 N S}{\gamma_2} \tag{3.48}$$

$$\frac{\partial \gamma_3}{\partial n_3} = \frac{k_0^2 (\mathrm{N S} - \mathrm{n}_3)}{\gamma_3} \tag{3.49}$$

$$\frac{\partial u}{\partial n_3} = \frac{[\gamma_3(j\sigma\omega - \gamma_3) k_0^2 N - \gamma_2^2 k_0^2 N \ ]S}{\gamma_2\gamma_3(j\sigma\omega - \gamma_3)^2} - \frac{\gamma_2 k_0^2 n_3}{\gamma_3(j\sigma\omega - \gamma_3)^2} \tag{3.50}$$

$$\frac{\partial u}{\partial n_3} = Y_1 S + Y_2 \tag{3.51}$$

$$Y_1 = \frac{(\gamma_3(j\sigma\omega - \gamma_3) k_0^2 N - \gamma_2^2 k_0^2 N \ )}{\gamma_2\gamma_3(j\sigma\omega - \gamma_3)^2} \tag{3.52}$$

$$Y_2 = \frac{\gamma_2 k_0^2 n_3}{\gamma_3(j\sigma\omega - \gamma_3)^2} \tag{3.53}$$

Differentiating Eq. (3.38)

$$\frac{\partial v}{\partial n_3} = \left(\frac{k_0^2 N}{\gamma_2\gamma_1 \sqrt{1 - \frac{\alpha k_0^2 E_z^2}{2\gamma_1^2}}} + \frac{k_0^2 N \ \gamma_2}{\gamma_0^3 \sqrt{1 - \frac{\alpha k_0^2 E_z^2}{2\gamma_1^2}}} + \frac{k_0^4 N \ \gamma_2 \ \alpha E_z^2}{2\gamma_0^5 \left(1 - \frac{\alpha k_0^2 E_z^2}{2\gamma_1^2}\right)^{1.5}} \right) S \tag{3.54}$$

$$\frac{\partial v}{\partial n_3} = Y_3 S \tag{3.56}$$

$$Y_3 = \left(\frac{k_0^{\,2} N}{\gamma_2 \gamma_1 \sqrt{1 - \frac{\alpha k_0^{\,2} E_z^{\,2}}{2\gamma_1^{\,2}}}} + \frac{k_0^{\,2} N \ \gamma_2}{\gamma_0^{\,3} \sqrt{1 - \frac{\alpha k_0^{\,2} E_z^{\,2}}{2\gamma_1^{\,2}}}} + \frac{k_0^{\,4} N \ \gamma_2 \ \alpha E_z^{\,2}}{2\gamma_0^{\,5} \left(1 - \frac{\alpha k_0^{\,2} E_z^{\,2}}{2\gamma_1^{\,2}}\right)^{1.5}} \right) \tag{3.57}$$

$$X_1 = u + v \tag{3.58}$$

$$X_2 = 1 - uv \tag{3.59}$$

which be written as

$$\frac{\partial R_1}{\partial n_3} = \frac{(Y_1 S + Y_2 + Y_3 S) X_2 - X_1(-Y_1 S v - Y_2 v) - X_1(-Y_3 S u)}{X_2^{\,2}} \tag{3.60}$$

$$\frac{\partial R_2}{\partial n_3} = \frac{(X_2 Y_1 + Y_3 X_2 + Y_1 v X_1 + X_1 Y_3 u) S}{X_2^{\,2}} + \frac{Y_2 X_2 + Y_2 v X_1}{X_2^{\,2}} \tag{3.61}$$

$$\frac{\partial R_1}{\partial n_3} - \frac{\partial R_2}{\partial n_3} = 0 \tag{3.62}$$

$$ZS - \frac{(X_2 Y_1 + Y_3 X_2 + Y_1 v X_1 + X_1 Y_3 u) S}{X_2^{\,2}} - \frac{(Y_2 X_2 + Y_2 v X_1)}{X_2^{\,2}} = 0 \tag{3.63}$$

$$\left(\frac{Z X_2^{\,2} - (X_2 Y_1 + Y_3 X_2 + Y_1 v X_1 + X_1 Y_3 u)}{X_2^{\,2}} \right) S = \frac{(Y_2 X_2 + Y_2 v X_1)}{X_2^{\,2}} \tag{3.64}$$

After some mathematical manipulations, we get:

$$S = \frac{(Y_2 X_2 + Y_2 v\, X_1)}{Z\, X^2{}_2 - (X_2 Y_1 + Y_3 X_2 + Y_1 v\, X_1 + X_1 Y_3 u)} \qquad (3.65)$$

3.5 Results and Discussion

The dispersion relation given by Eq. (3.35) is solved numerically for the effective index *N*. This value is then substituted in Eq. (3.65) to find the sensitivity.

All the media are considered to be nonmagnetic, $\mu_0 = \mu_2 = \mu_3 = 1$ so we obtaine, $r = \frac{\alpha E^2}{2}$, which is a nonlinear factor .

Figure (3.2) shows the real effective index (*N*) from Eq. (3.34) for TE_0 as a function of angular frequency at different values of *d* (the thickness of dielectric layer). The graphene conductivity $\sigma_0 = 6.085 \times 10^{-5} siemens$, the nonlinear factor (r) is fixed to 0.1, and the frequency is taken in Terahertz range. As the thickness of the dielectric layer increases, the real effective index (*N)* decreases. Additionally, increasing the angular frequency, the real part of the effective index *(N*) increases.

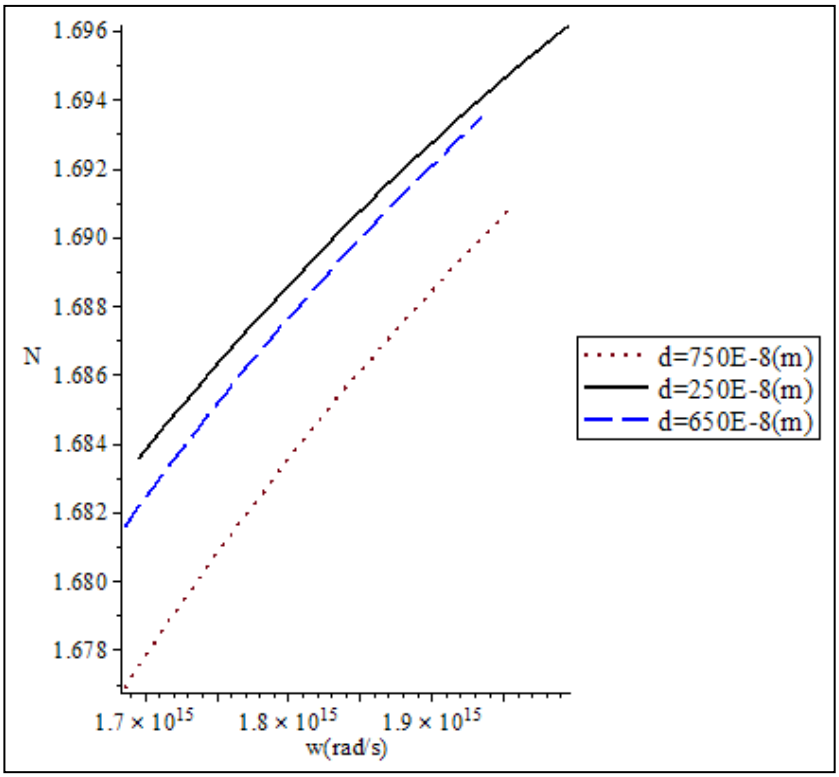

Figure (3.2): The effective index (*N*) of TE_0 versus from angular frequency for different thickness *d (m)* at nonlinear factor *r*=0.1, and conductivity of grapheme, $\sigma_0 = 6.085\times10^{-5}$ *siemens.*

The real effective index (*N*) for TE_1 versus angular frequency at different values of thickness is plotted in Figure. In the calculating The graphene conductivity $\sigma_0 = 6.085\times10^{-5}$ *siemens.* The nonlinear factor (*r*) is fixed to 0.1, and the angular frequency is taken in Terahertz. In Figure(3.3), it is noticeable that *N* depend on d values As the thickness of the dielectric layer increases, the real effective index (*N*) also increases. Moreover, increasing the frequency, the real part of the effective index (*N*) increases

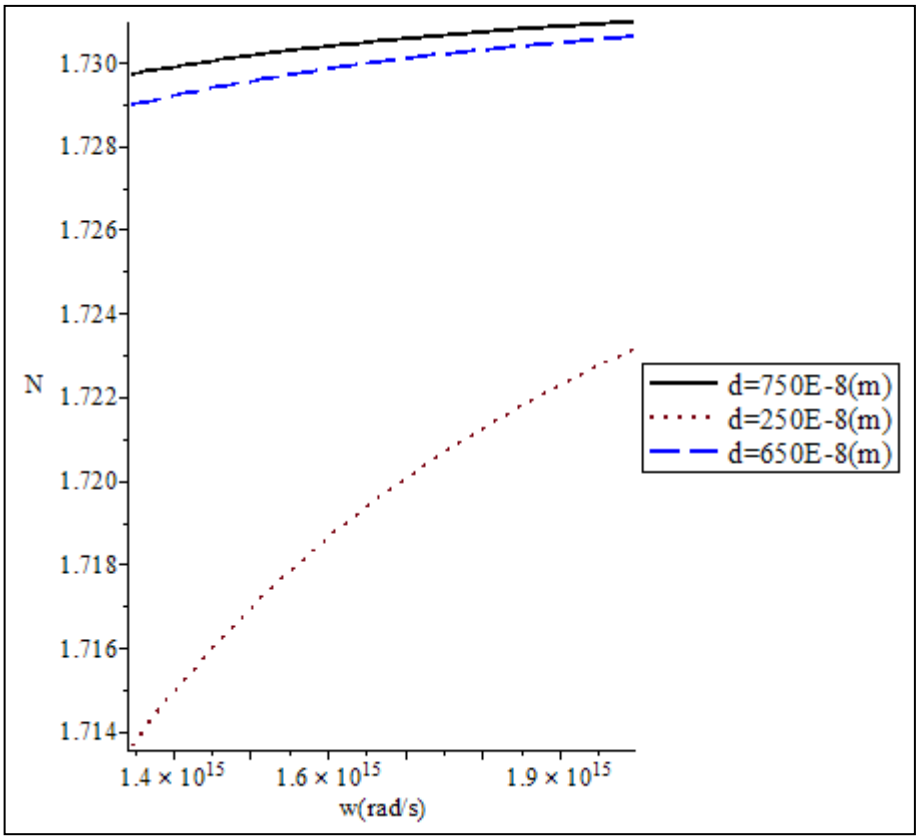

Figure (3.3): The effective index (*N*) of TE_1 versus from as function of angular frequency for different values of *d*, a nonlinear factor r=0.1, and conductivity of grapheme, $\sigma_0 = 6.085\times10^{-5}$ *siemens.*

Figure (3.4) illustrates the relation between the effective index (*N*) of the TE_0 mode at the thickness $d=280\times10^{-8}(m)$ for different values of nonlinear factor ***r*.** It can be seen that the real effective index (*N*) gets higher with inecreasing nonlinear factor. It can be seen that from Figer (3.4) that the real effective index (*N*) starts its values from: 1.65 to 1.681 for the values of r versuse of r varies from *0.1 to 0.5*. The conductivity of graphene $\sigma_0 = 6.085\times10^{-7}\, siemens$**.**

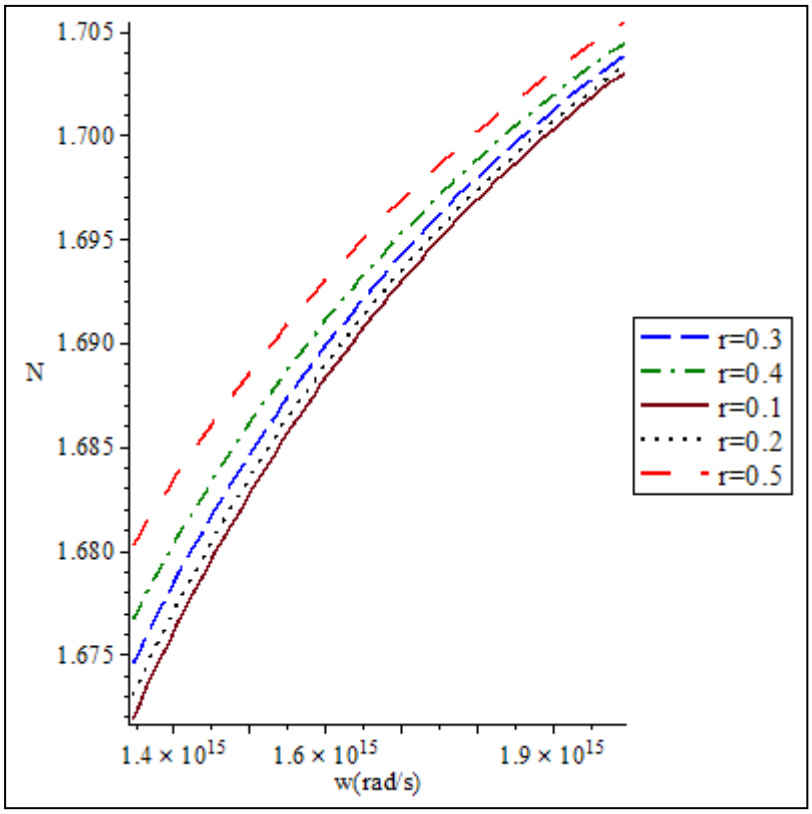

.

Figure (3.4): The effective index *(N)* for TE_0 versus angular frequency at thickness dielectric layer, $d=280\times10^{-8}(m)$ for different ***r*,** mode order at *m=0*, and conductivity of grapheme, $\sigma_0 = 6.085\times10^{-7}\, siemens.$

Figure (3.5) displays effective index of the proposed waveguide structure versus frequency for fundamental mode TE_0 at different values of r (positive and negative) the negative r is a little increasing effective index from positive r ,for fixed $d=250\times10^{-8}(m)$ and conductivity of graphene $\sigma_0 = 6.085\times10^{-7}\, siemens$.

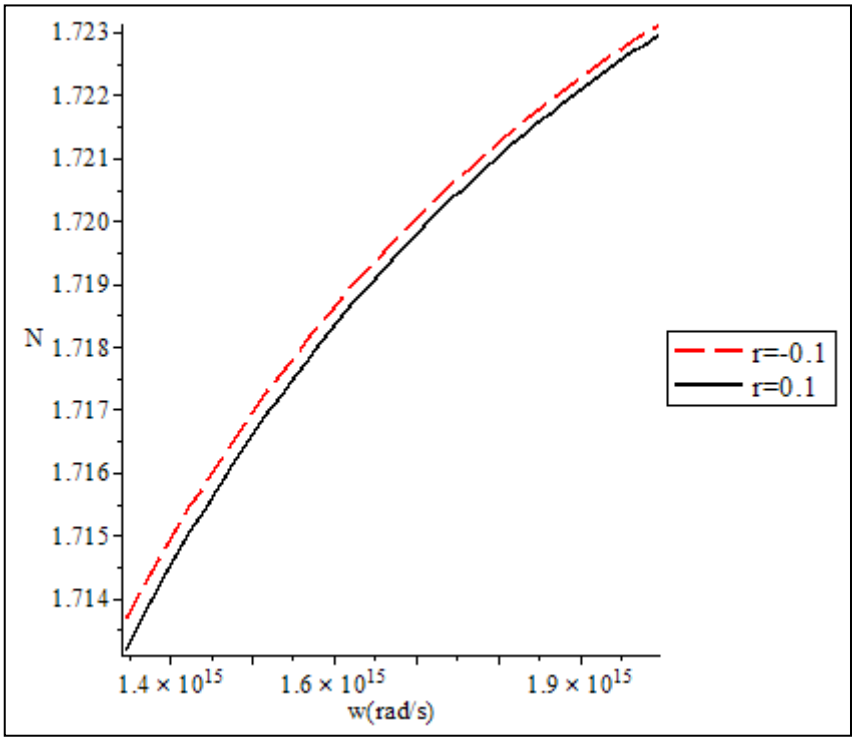

Figure (3.5): The effective index (N) for TE_0 against the frequency for thickness dielectric layer, $d=280\times10^{-8}(m)$ for different r, mode order at $m=0$, and conductivity of graphene $\sigma_0 = 6.085\times10^{-7}\, siemens$.

Figure (3.6) shows the effect of changing mode *m* (0, 1) on the effective index *(N)* versus frequency. For *m=1* the effective index has higher values than for *m=0*. For *m=1*, the values of *N* is hardly change. In the calculation, the values of *d*, *r* and σ kept constants. They are assumed to have the following values: $d=250\times10^{-8}(m), \sigma_0 = 6.085\times10^{-7}\ siemens$, and *r*=0.1.

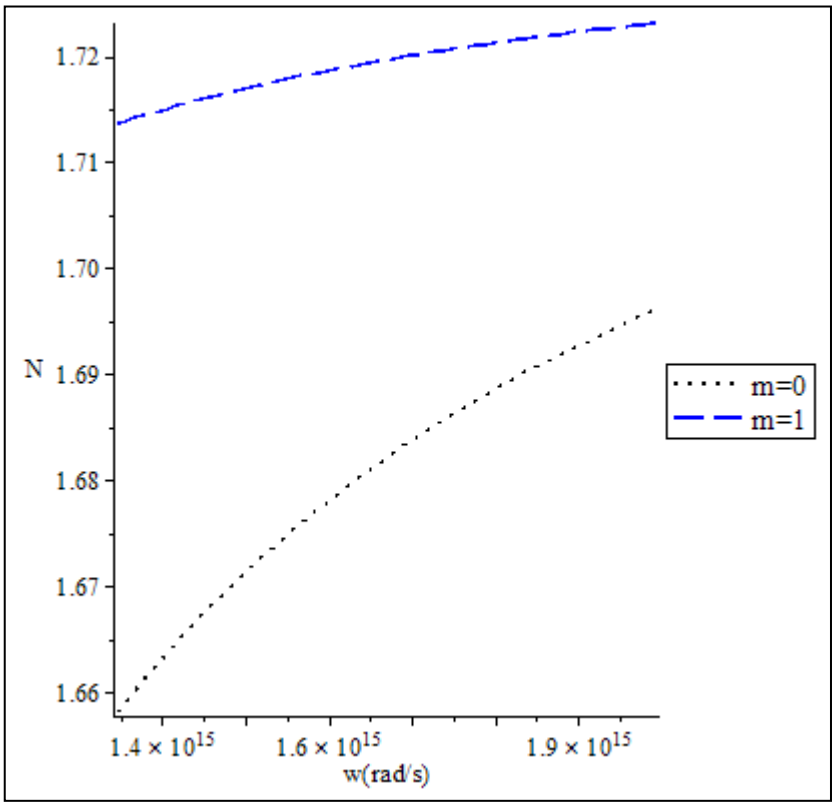

Figure (3.6): The effective index *(N)* versus the frequency thickness dielectric layer, $d=250\times10^{-8}(m)$ for different *m* mode order at *r*=0.1, and $\sigma_0 = 6.085\times10^{-7}\ siemens$.

Results and discussions of sensitivity

The sensitivity versus the real part of N is plotted in Figure (3.7) for different nonlinear factor, at layer thickness, $d=650\times10^{-8}(m)$ for TE_1 and $\sigma_0 = 6.085\times10^{-6}\,siemens$.

It is clear from Figure (3.7) that the sensitivity of the structure increasing with the nonlinear factor. The sensitivity of the structure increasing to reach a peak then values decreases as the real part of *N* increases. Upon plotting

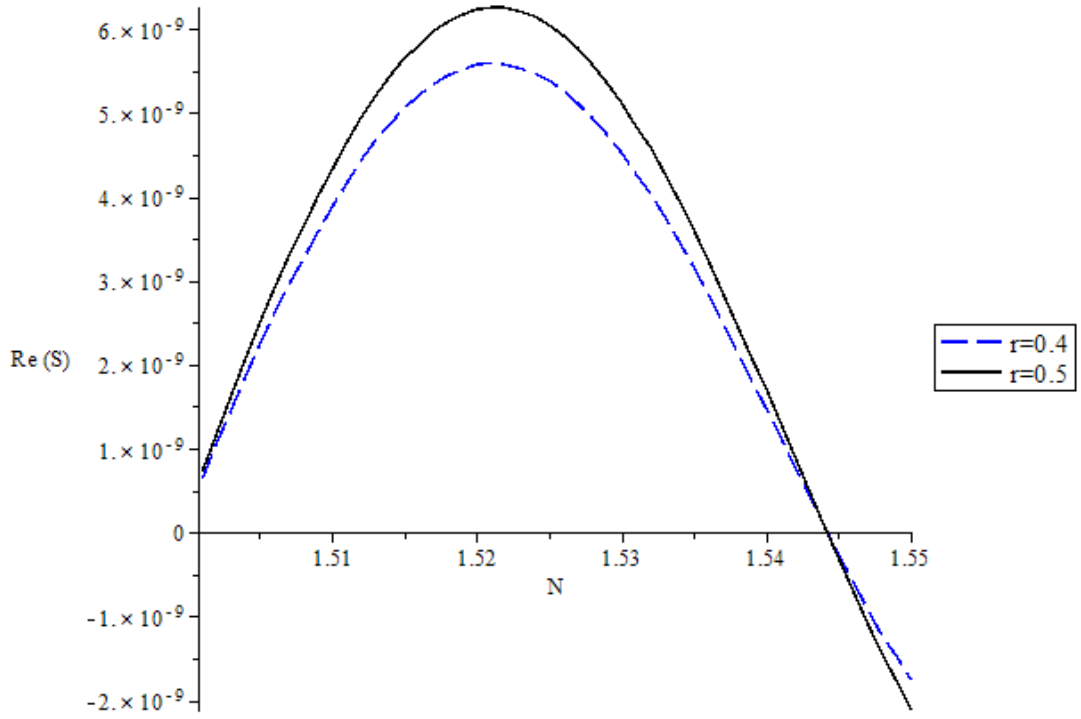

Figure (3.7): The real part of the sensitivity versus the real effective index (*N*) for different values of r at thickness of dielectric layer, $d=650\times10^{-8}(m)$ for m=1 TE_1 and $\sigma_0 = 6.085\times10^{-6}\,siemens$.

Figures (3.8) presents the relationship between the real part of the sensitivity of the proposed sensor and effective index (N) for different positive values of the nonlinear factor (r) positive. It is clear from Figures (3.8), that an increase of the effective index (N) and decrease of nonlinear factor (r), would result in an increasing of the peak. The sensitivity value cut off is at the same value of effective index (N) and peak at the some value of effective index (N) for the different values of the nonlinear factor(r).

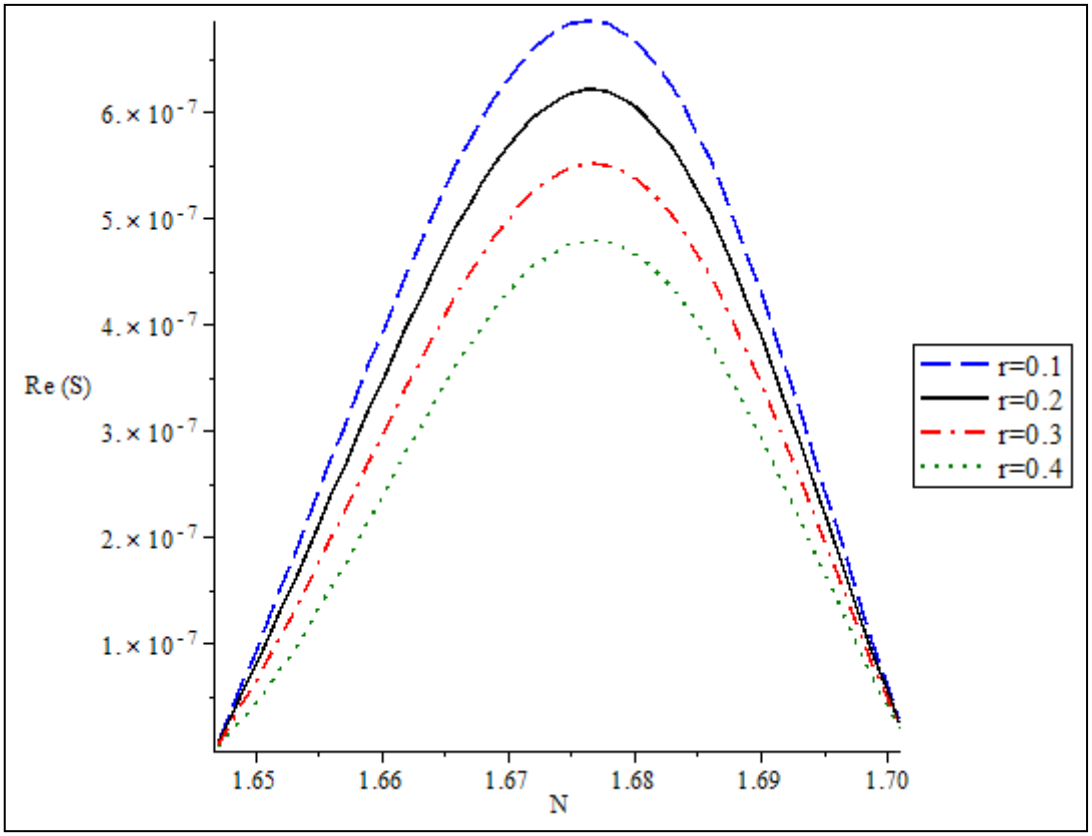

Figure (3.8): The real part of the sensitivity versus the real effective index (N) for different values of r at thickness of dielectric layer, $d=250\times10^{-8}(m)$ for m=1 TE_1 and $\sigma_0 = 6.085\times10^{-7}\, siemens$.

Figures (3.9) illustrates the relationship between the real part of the sensitivity of the proposed sensor and effective index (N) for different values of the negative nonlinear factor (r). It is clear from Figures (3.9) that an increase in both the effective index (N) and nonlinear factor (r), would result in an increasing value of the peak.

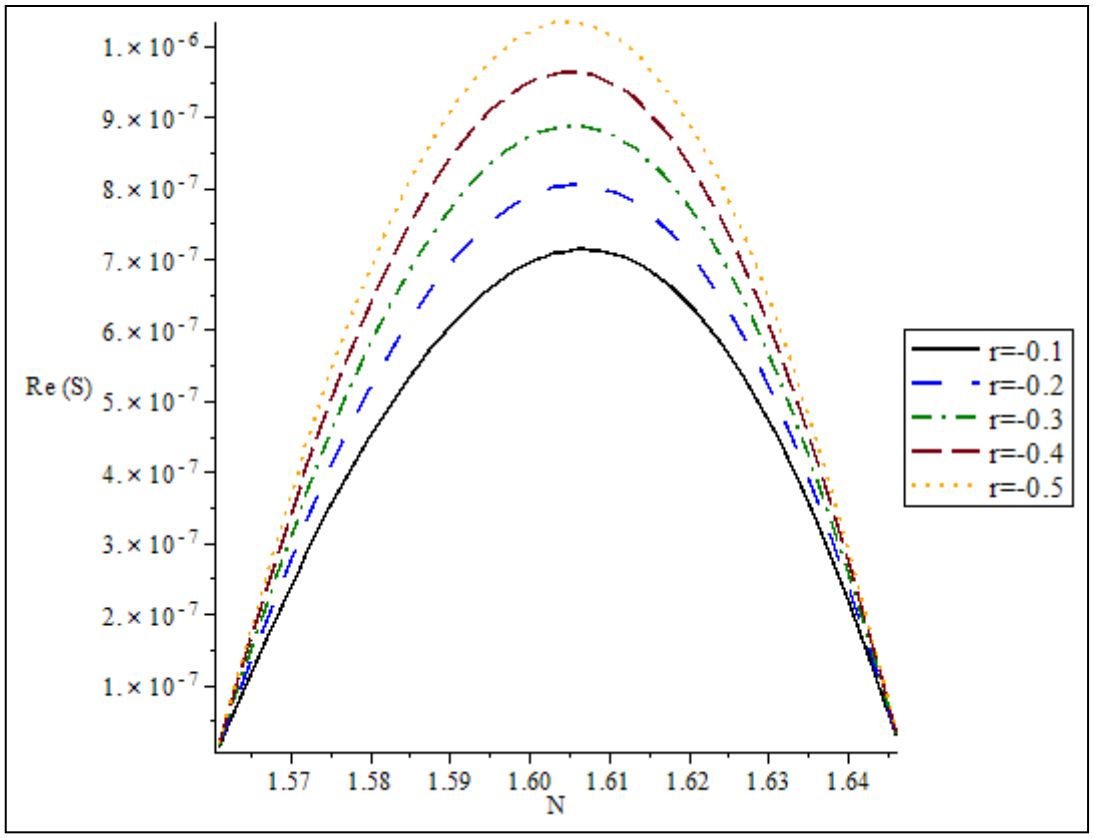

Figure (3.9): The real part of the sensitivity versus the real effective index (N) for different values of $-r$ at thickness of dielectric layer, $d=250\times10^{-8}(m)$ for m=1 TE_1 and $\sigma_0 = 6.085\times10^{-7}\, siemens$.

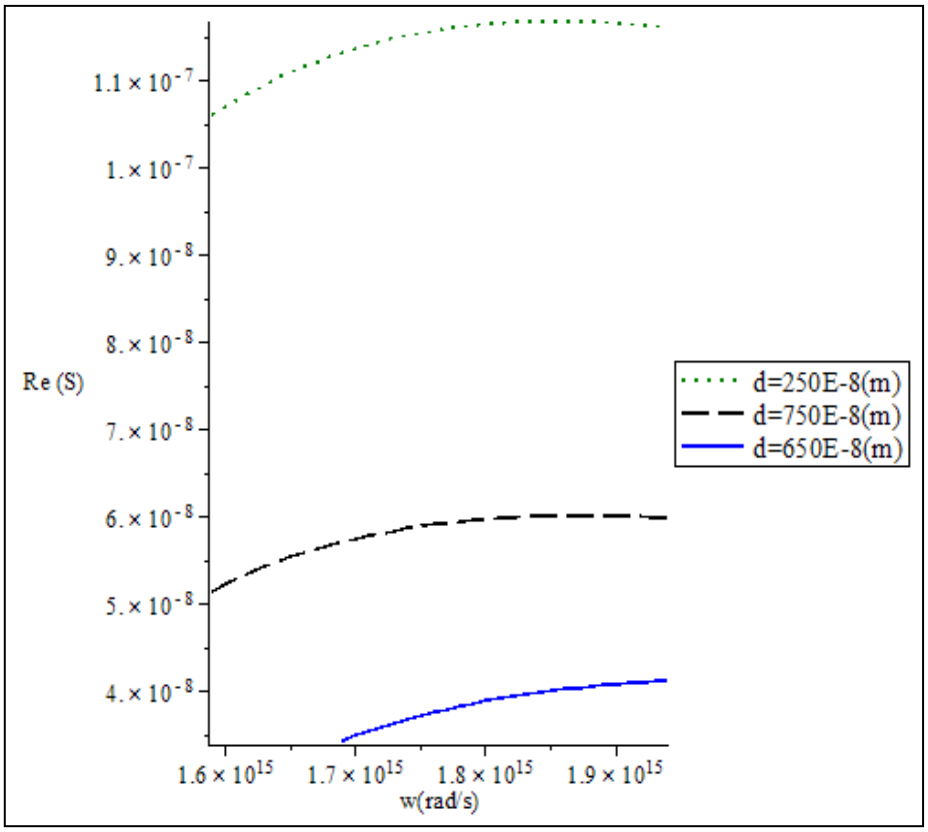

Figure (3.10): The real part of the sensitivity versus the frequency (ω) for different values of the thickness of the dielectric layer, r=0.5, m=1 and $\sigma_0 = 6.085\times10^{-7}\, siemens$.

It can be seen from Figure (3.10) that the sensitivity increases with increasing the angular frequency. Moreover, the sensitivity is highest at $d=250\times10^{-8}(m)$ and lowest at $d=650\times10^{-8}(m)$and at $d=750\times10^{-8}(m)$ between them.

A comparison between *TE* guided modes is carried out in Figures (3.11) and (3.12) where the real part of the sensitivity of the proposed sensor is plotted against nonlinear factor. We found that when $m=0$, $d=650\times10^{-8}(m)$ produces given negative value however when m=1,$d=650\times10^{-8}(m)$ gives positive while for $d=250\times10^{-8}(m)$ and $750\times10^{-8}(m)$,we get negatives values when $m=0$ and positves values when m=1.

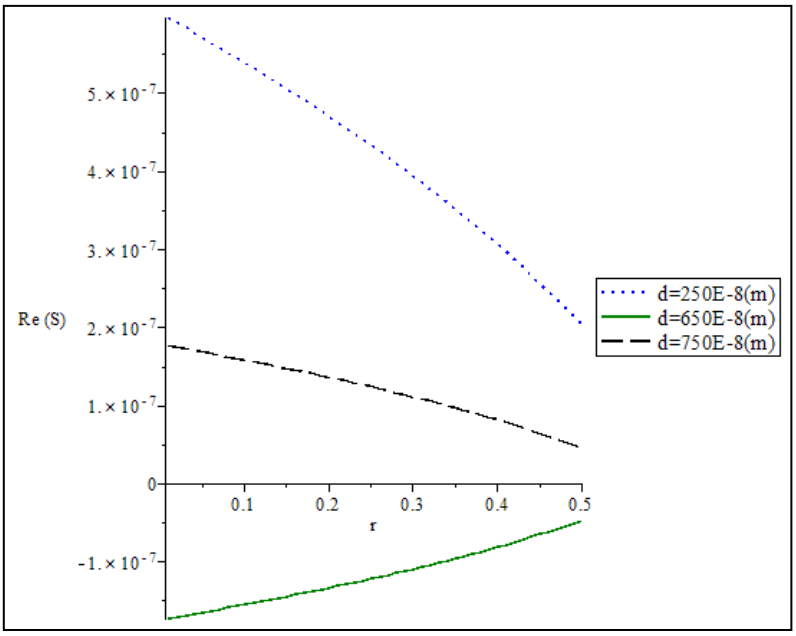

Figure (3.11): The real part of the sensitivity versus then nonlinear factor (*r*) for different values of the thickness of the dielectric layer (*d*), *m*=0, ω =1.756×10^{15}(Hz) and $\sigma_0 = 6.085\times10^{-7}$ *siemens*.

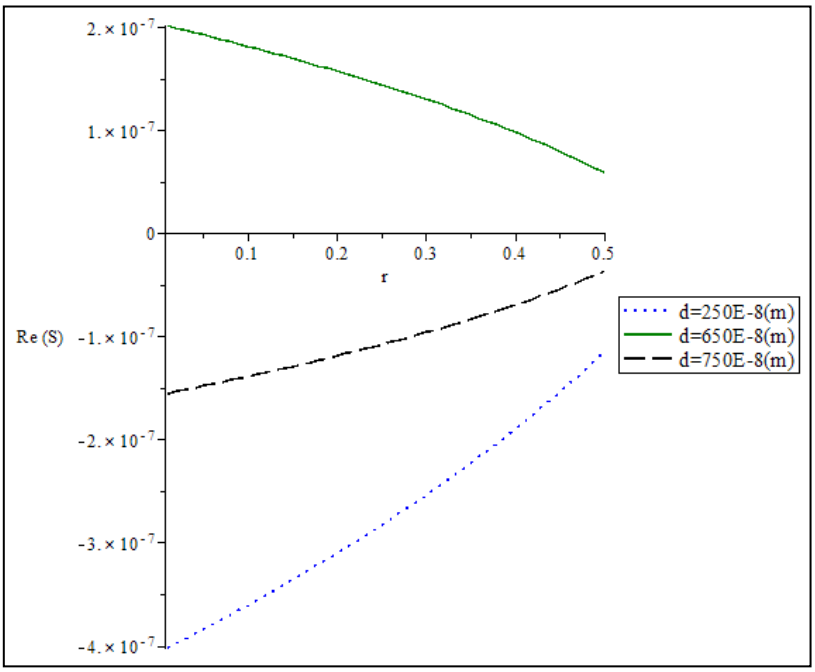

Figure (3.12): The real part of the sensitivity versus then nonlinear factor (*r*) for different values of the thickness of the dielectric layer *(d)*, *m*=1, ω =1.756×10^{15}(Hz) $\sigma_0 = 6.085\times10^{-7}$ *siemens*.

Figures (3.13), (3.14) and (3.15) exhibit the real part of the sensitivity of the proposed sensor versus the frequency for different values of the conductivity of graphene. It can be seen from these Figures that the sensitivity increases to peak then decreases with increasing the frequency. In addition, the highest value of the sensitivity is obtained when the value of the conductivity of grapheme, $\sigma_0 = 6.085\times10^{-7}\, siemens$.

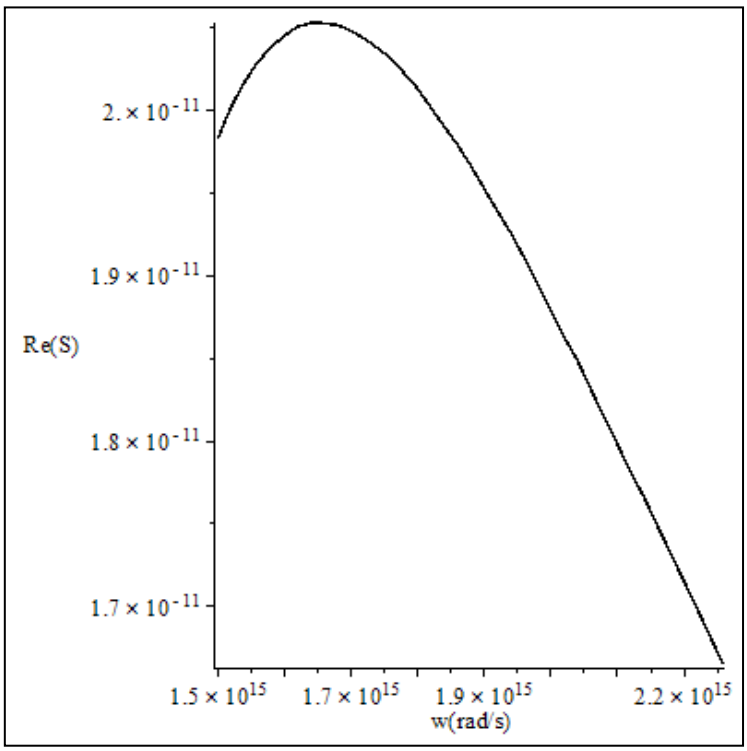

Figure (3.13): The real part of the sensitivity versus the frequency (ω) for values of $d=250\times10^{-8}(m)$, $r=0.5$, $m=0$ and $\sigma_0 = 6.085\times10^{-5}\, siemens$.

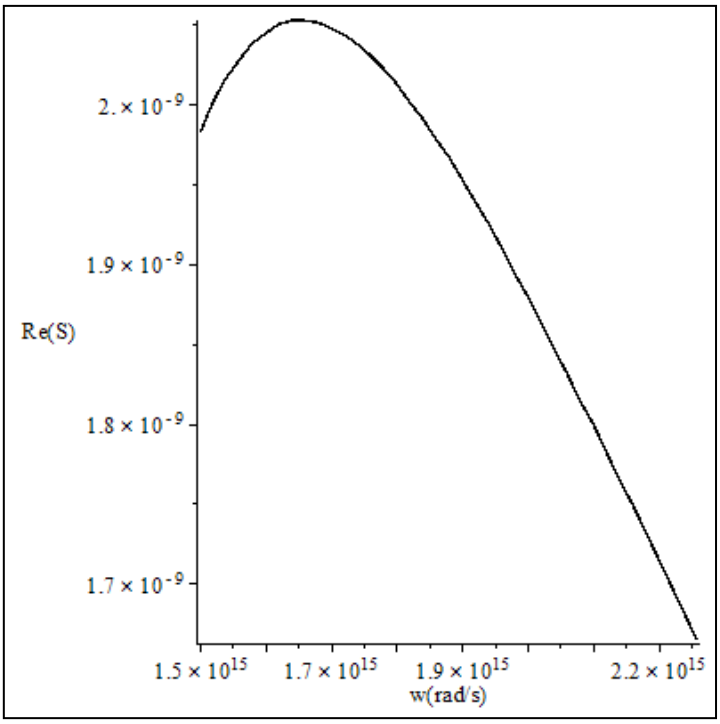

Figure (3.14): The real part of the sensitivity versus the frequency (ω) for values of d=250×10^{-8}(m), r=0.5, m=0, $\sigma_0 = 6.085\times10^{-6}$ *siemens*.

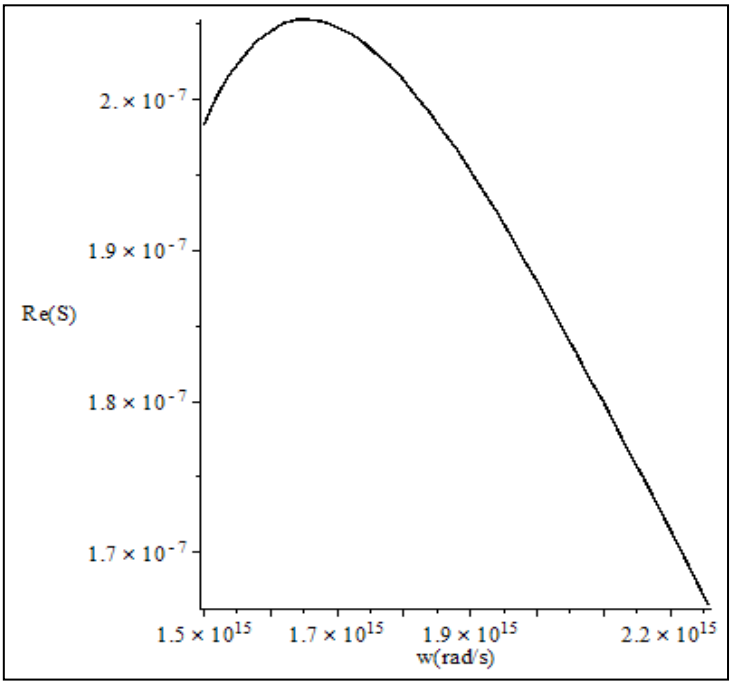

Figure (3.15): The real part of the sensitivity versus the frequency (ω) for values of d=250×10^{-8} (m), r=0.5, m=0 and $\sigma_0 = 6.085\times10^{-7}$ *siemens*.

Chapter 4

Conclusion

Conclusion

In this thesis, the main purpose is to study a structure of optical waveguide sensor, three layers waveguide sensor for sensing at various physical parameters. We analyses three layers waveguide sensor when the propagation of TE- polarized waves in a slab waveguide structure support with nonlinear layer substrate. One of the layers is considered as an infinitesimally thin of graphene material.

Our results are important for a better understanding of Graphene of TE- polarized waves with nonlinear layer, which are useful to design the various graphene-bases optoelectronic devices.

In conclusion, we have:

- The real part of the effective index *Re(N),* versus as a function of angular frequency at different values of *d* (the thickness of dielectric layer). *Re(N)* increases with increasing the value of angular frequency and decreasing *d* at TE_0 .
- Re (*N*) increases with increasing the mode order and gets more higher values with TE_1 mode more than TE_0.
- The relation between the effective index (*N*) of the TE_0 mode at fixed thickness *d* for different nonlinear factor *r* values increasing should that Re (*N*) with increasing *r*.
- The negative r produce a little increasing effective index than positive r.
- When the real part of the sensitivity of the proposed sensor is plotted versus the real effective index (*N*) for different values of *r*, the sensitivity increasing with decreasing positive nonlinear factor r and increasing negative nonlinear factor *r* at $d=250\times10^{-8}(m)$.
- The sensitivity increases with increasing the angular frequency that the sensitivity is maximum at $d=250\times10^{-8}\ (m)$ and minimum at $d=650\times10^{-8}\ (m)$.
- At different TE_0 and TE_1 the sign of sensitivity is changing.
- The sensitivity has the highest values for conductivity of grapheme, $\sigma_0 = 6.085\times10^{-7}\ siemens$.

The Reference List

The Reference List

Bae, S., Kim, H., Lee, Y., Xu, X., Park, J. S., Zheng, Y., et al. (2010). Roll-to-roll production of 30-inch graphene films for transparent electrodes. *Nature nanotechnology*, *5*(8), 574-578.

Blake, L. V. (1969). *Transmission lines and waveguides*.

Blake, P., Hill, E. W., Neto, A. C., Novoselov, K. S., Jiang, D., Yang, R., et al. (2007). Making graphene visible. *Applied Physics Letters*, *91*(6), 063124.

Bludov, Y. V., Ferreira, A., Peres, N. M. R., & Vasilevskiy, M. I. (2013). A primer on surface plasmon-polaritons in graphene. *International Journal of Modern Physics B*, *27*(10), 1341001.

Bonaccorso, F., Sun, Z., Hasan, T., & Ferrari, A. C. (2010). Graphene photonics and optoelectronics. *Nature photonics*, *4*(9), 611-622.

Born, M., & Wolf, E. (2000). *Principles of optics: electromagnetic theory of propagation, interference and diffraction of light*. CUP Archive..

Bunch, J. S. (2008). *Mechanical and electrical properties of graphene sheets*(Doctoral dissertation, Cornell University).

Casiraghi, C., Hartschuh, A., Lidorikis, E., Qian, H., Harutyunyan, H., Gokus, T., Ferrari, A. C. (2007). Rayleigh imaging of graphene and graphene layers. *Nano letters*, *7*(9), 2711-2717.

Chen, C. L. (1996). *Elements of optoelectronics and fiber optics*. Richard d Irwin.

Chen, C. L. (2006). *Foundations for guided-wave optics*. John Wiley & Sons.

Cherin, A. H. (1983). *An Introduction To Optical Fibers*.

Christensen, J., Manjavacas, A., Thongrattanasiri, S., Koppens, F. H., & García de Abajo, F. J. (2011). Graphene plasmon waveguiding and hybridization in individual and paired nanoribbons. *ACS nano*, *6*(1), 431-440.

Dienwiebel, M., Verhoeven, G. S., Pradeep, N., Frenken, J. W., Heimberg, J. A., & Zandbergen, H. W. (2004). Superlubricity of graphite. *Physical Review Letters*, *92*(12), 126101.

Dragoman, M., Neculoiu, D., Dragoman, D., Deligeorgis, G., Konstantinidis, G., Cismaru, A., ... & Plana, R. (2010). Graphene for microwaves. *IEEE microwave magazine*, *11*(7), 81-86.

Dresselhaus, M. S., & Dresselhaus, G. (2002). Intercalation compounds of graphite. *Advances in physics*, *51*(1), 1-186.

El-Khozondar, H. J., El-Khozondar, R. J., & Shabat, M. M. (2007, October). Temperature stress effects on optical nonlinear waveguide sensor. In*International Symposium on Optomechatronic Technologies* (pp. 67160B-67160B). International Society for Optics and Photonics.

El-Khozondar, H., El-Khozondar, R., Zouhdi, S.,2015a. tunable MTMs consists of a singlr-walled nanotube thin filme waveguide covered by nonlinear cladding. Applied Physics A, 119(2),451-453.

El-Khozondar, H., El-Khozondar, R., Shabat, M.,2015b. Metamaterial-Dielectric Photonics crystal waveguide structure. Optics special Issue : optical Engineering of Applications,4(1-2),1-4.

El-Khozondar, H., El-Khozondar, R., Zouhdi, S.,2014. Propagation of surface wave at the interface between nonlinear MTMs and Anisotropic Matrials, Applied Physics A, 115 (2),439-442.

El-Khozondar, H., El-Khozondar, R., Shabat, M., koch,A.,2012a. TM waves propagation at magnetoplasma-MTMs interface, world of Condensed Matter Physics, 2(4), 171-174.

El-Khozondar, H., El-Khozondar, R., Zouhdi, S.,2012b. Surface Waves at the interface between tunable LC-MTMs and nonlinear media, Applied Physics A., 109(4), 865-867.

El-Khozondar, H., El-Khozondar, R., Shabat, M., 2011. Surface wave propagation

Further research on sensors have been presented. El-Saifi et al., 2004 have studied Band reject filter of a periodic dielectric film bounded by a nonlinear cladding.

El-Khozondar, H., El-Khozondar, R., Shabat, M., koch,A.,2007. Stress effect on optical nonlinear waveguide sensor . Journal of optical communication, 28(3), 35-47.

El-Khozondar, H., El-Khozondar, R., Shabat, M.,2008b. Temperature enhancement oh nonlinear optical channel waveguide sensors using thermal-stress effect, Islamic university Journal for Natural science and Engineering,16(2),9-20.

El-Khozondar et al. (2016) of sensor comprised of single layer graphene inserted between matamaterial and dielectric media. They exhibited that the sensitivity depends on the MTMparameters.

El-Khozondar et al.(2017a) have demensotrated a new sensor configuration made of graphene at distance from plasma substrate.

El-Khozondar et al.(2017b) have derived the dispersion relation of the travelling TM surface plasmain the sensor structure include a graphene layer. They noticed that the MTM Paramaters can control the propagation of the plasmon.

Evans, J. W., Thiel, P. A., & Bartelt, M. C. (2006). Morphological evolution during epitaxial thin film growth: Formation of 2D islands and 3D mounds.*Surface Science Reports*, *61*(1), 1-128.

Excelatphysics. (2014). *Total-Internal-Reflection*. Retrieved April 20, 2016, from: http://www.excelatphysics.com/total-internal-reflection.html**.**

Geim, A. K., & Novoselov, K. S. (2007). The rise of graphene. *Nature materials*, *6*(3), 183-191.

Griffiths, D. J. (1999). Introduction to electrodynamics. *Prentice Hall*, *93*, 95.

Gusynin, V. P., Sharapov, S. G., & Carbotte, J. P. (2006). Magneto-optical conductivity in graphene. *Journal of Physics: Condensed Matter*, *19*(2), 026222.

Hamada, M. S., Shabat, M. M., & El-Amassi, D. M. (2015). Design of Novel Graphene-Waveguide Sensor. *Sensor Letters*, *13*(9), 764-768.

Hanson, G. W. (2008). Dyadic Green's functions and guided surface waves for a surface conductivity model of graphene. *Journal of Applied Physics*, *103*(6), 064302.

Horiuchi, S., Gotou, T., Fujiwara, M., Asaka, T., Yokosawa, T., & Matsui, Y. (2004). Single graphene sheet detected in a carbon nanofilm. *Applied physics letters*, *84*(13), 2403-2405.

Hunsperger, R. G. (2009). Optical Waveguide Modes. In *Integrated Optics* (pp. 17-31). Springer New York.

Hunsperger, R. G., & Meyer-Arendt, J. R. (1992). Integrated optics: theory and technology. *Applied Optics*, *31*, 298.

Jackson, J. D. (1999). *Classical electrodynamics*. Wiley.

Jo, G., Choe, M., Cho, C. Y., Kim, J. H., Park, W., Lee, S., ... & Kahng, Y. H. (2010). Large-scale patterned multi-layer graphene films as transparent conducting electrodes for GaN light-emitting diodes. *Nanotechnology*, *21*(17), 175201.

Ju, L., Geng, B., Horng, J., Girit, C., Martin, M., Hao, Z., et al. (2011). Graphene plasmonics for tunable terahertz metamaterials. *Nature nanotechnology*, *6*(10), 630-634.

Kawano, K., & Kitoh, T. (2001). *Frontmatter and Index* (pp. i-xviii). John Wiley & Sons, Inc.

Iizuka, K. (2002). Elements of Photonics, Volume II: For Fiber and Integrated Optics. Keigo Iizuka Copyright . John Wiley & Sons, Inc.

Kenji, K., & Tsutomu, K. (2001). Introduction to optical waveguide analysis.

Khorasani, S., & Rashidian, B. (2001). Guided light propagation in dielectric slab waveguide with conducting interfaces. *Journal of Optics A: Pure and Applied Optics*, *3*(5), 380.

Kuzmenko, A. B., Van Heumen, E., Carbone, F., & Van Der Marel, D. (2008). Universal optical conductance of graphite. *Physical review letters*, *100*(11), 117401.

Landau, L. D. (1937). Zur Theorie der phasenumwandlungen II. *Phys. Z. Sowjetunion*, *11*, 26-35.

Landau, L. D., & Lifshitz, E. M. (1980). Statistical Physics, 3rd. *Edition (Part 1 Oxford: Pergamon Press. 1980).*

Li, Z. Q., Henriksen, E. A., Jiang, Z., Hao, Z., Martin, M. C., Kim, P., et al. (2008). Dirac charge dynamics in graphene by infrared spectroscopy. *Nature Physics*, *4*(7), 532-535.

Liu, M., Yin, X., Ulin-Avila, E., Geng, B., Zentgraf, T., Ju, L., et al. (2011). A graphene-based broadband optical modulator. *Nature*, *474*(7349), 64-67.

Liu, Y., Willis, R. F., Emtsev, K. V., & Seyller, T. (2008). Plasmon dispersion and damping in electrically isolated two-dimensional charge sheets. *Physical Review B*, *78*(20), 201403.

Lorrain, P., & Corson, D. (1970). Electromagnetic fields and waves.

Maier, S. A. (2007). *Plasmonics: fundamentals and applications*. Springer Science & Business Media.

Mak, K. F., Sfeir, M. Y., Wu, Y., Lui, C. H., Misewich, J. A., & Heinz, T. F. (2008). Measurement of the optical conductivity of graphene. *Physical review letters*, *101*(19), 196405.

Markos, P., & Soukoulis, C. M. (2008). *Wave propagation: from electrons to photonic crystals and left-handed materials*. Princeton University Press.

Marshall, S. V., & Skitek, G. G. (1990). *Electromagnetic concepts and applications*.

Mermin, N. D. (1968). Crystalline order in two dimensions. *Physical Review*,*176*(1), 250.

Meyer, J. C., Geim, A. K., Katsnelson, M. I., Novoselov, K. S., Booth, T. J., & Roth, S. (2007). The structure of suspended graphene sheets. *Nature*,*446*(7131), 60-63.

Mikhailov, S. A., & Ziegler, K. (2007). New electromagnetic mode in graphene. *Physical Review Letters*, *99*(1), 016803.

Morozov, S. V., Novoselov, K. S., Schedin, F., Jiang, D., Firsov, A. A., & Geim, A. K. (2005). Two-dimensional electron and hole gases at the surface of graphite. *Physical Review B*, *72*(20), 201401.

Nair, R. R., Blake, P., Grigorenko, A. N., Novoselov, K. S., Booth, T. J., Stauber, T., et al. (2008). Fine structure constant defines visual transparency of graphene. *Science*, *320*(5881), 1308-1308.

Neto, A. C., Guinea, F., Peres, N. M., Novoselov, K. S., & Geim, A. K. (2009). The electronic properties of graphene. *Reviews of modern physics*, *81*(1), 109.

Nikitin, A. Y., Guinea, F., García-Vidal, F. J., & Martín-Moreno, L. (2011). Edge and waveguide terahertz surface plasmon modes in graphene microribbons.*Physical Review B*, *84*(16), 161407.

Novoselov, K. S., Geim, A. K., Morozov, S. V., Jiang, D., Zhang, Y., Dubonos, S. V., et al. (2004). Electric field effect in atomically thin carbon films. *science*, *306*(5696), 666-669.

Novoselov, K. S., Jiang, D., Schedin, F., Booth, T. J., Khotkevich, V. V., Morozov, S. V., & Geim, A. K. (2005). Two-dimensional atomic crystals.*Proceedings of the National Academy of Sciences of the United States of America*, *102*(30), 10451-10453.

Okamoto, K. (2006). Fundamentals of Optical Waveguides 2nd edn (New York: Academic).

Parriaux, O., & Dierauer, P. (1994). Normalized expressions for the optical sensitivity of evanescent wave sensors. *Optics letters*, *19*(7), 508-510.

Parriaux, O., & Veldhuis, G. J. (1998). Normalized analysis for the sensitivity optimization of integrated optical evanescent-wave sensors. *Journal of lightwave technology*, *16*(4), 573.

Partoens, B., & Peeters, F. M. (2006). From graphene to graphite: Electronic structure around the K point. *Physical Review B*, *74*(7), 075404.

Peierls, R. (1935). Quelques propriétés typiques des corps solides. In *Annales de l'institut Henri Poincaré* (Vol. 5, No. 3, pp. 177-222).

Pertsin, A., & Grunze, M. (2006). Water as a lubricant for graphite: A computer simulation study. *The Journal of chemical physics*, *125*(11), 114707.

Physics.stackexchange. (2006). *Propagation of an electromagnetic field*. Retrieved November 6, 2016, from: http://physics.stackexchange.com/questions/123805/on-the-shape-of-magnetic-and-electric-fields-in-an-electromagnetic-wave.

Pollock, C. R. (1995). Fundamentals of optoelectronics.

Pozar, D. M. (2009). *Microwave engineering*. John Wiley & Sons.

Raether, H. (1988). *Surface plasmons on smooth surfaces* (pp. 4-39). Springer Berlin Heidelberg.

Sadiku, M. N. (2001). *Elements of electromagnetics* (Vol. 428). New York: Oxford university press.

Saito, R., Dresselhaus, G., & Dresselhaus, M. S. (1998). *Physical properties of carbon nanotubes* (Vol. 35). London: Imperial college press.

Savage, R. H. (1948). Graphite lubrication. *Journal of applied physics*, *19*(1), 1-10.

Shabat, M. M., Khalil, H., Taya, S. A., & Abadla, M. M. (2007). Analysis of the sensitivity of self-focused nonlinear optical evanescent waveguide sensors.*International Journal of Optomechatronics*, *1*(3), 284-296.

Shioyama, H. (2001). Cleavage of graphite to graphene. *Journal of materials science letters*, *20*(6), 499-500.

Snyder, A. W., & Love, J. (2012). *Optical waveguide theory*. Springer Science & Business Media.

Stankovich, S., Dikin, D. A., Dommett, G. H., Kohlhaas, K. M., Zimney, E. J., Stach, E. A., et al. (2006). Graphene-based composite materials.*nature*, *442*(7100), 282-286..

Stauber, T., & Gómez-Santos, G. (2012). Plasmons and near-field amplification in double-layer graphene. *Physical Review B*, *85*(7), 075410.

Stauber, T., Peres, N. M. R., & Geim, A. K. (2008). Optical conductivity of graphene in the visible region of the spectrum. *Physical Review B*, *78*(8), 085432.

Sun, Z., Hasan, T., Torrisi, F., Popa, D., Privitera, G., Wang, F., et al. (2010). Graphene mode-locked ultrafast laser. *ACS nano*, *4*(2), 803-810.

Taya, S. A., & Shabat, M. M. (2011). Sensitivity enhancement in optical waveguide sensors using metamaterials. *Applied Physics A*, *103*(3), 611-614.

Taya, S. A., El-Agez, T. M., Kullab, H. M., Abadla, M. M., & Shabat, M. M. (2012). Theoretical study of slab waveguide optical sensor with left-handed material as a core layer. *Optica applicata*, *42*(1), 193-205.

Taya, S. A., Shabat, M. M., & Khalil, H. M. (2009). Enhancement of sensitivity in optical waveguide sensors using left-handed materials. *Optik-International Journal for Light and Electron Optics*, *120*(10), 504-508.

Taya, S. A., Shabat, M. M., Khalil, H. M., & Jäger, D. S. (2008). Theoretical analysis of TM nonlinear asymmetrical waveguide optical sensors. *Sensors and Actuators A: Physical*, *147*(1), 137-141.

Thongrattanasiri, S., Koppens, F. H., & de Abajo, F. J. G. (2012). Complete optical absorption in periodically patterned graphene. *Physical review letters*,*108*(4), 047401.

Vakil, A., & Engheta, N. (2011). Transformation optics using graphene.*Science*, *332*(6035), 1291-1294.

Venables, J. A., Spiller, G. D. T., & Hanbucken, M. (1984). Nucleation and growth of thin films. *Reports on Progress in Physics*, *47*(4), 399.

Viculis, L. M., Mack, J. J., & Kaner, R. B. (2003). A chemical route to carbon nanoscrolls. *Science*, *299*(5611), 1361-1361.

Wang, B., Zhang, X., García-Vidal, F. J., Yuan, X., & Teng, J. (2012). Strong coupling of surface plasmon polaritons in monolayer graphene sheet arrays.*Physical review letters*, *109*(7), 073901.

Wang, F., Zhang, Y., Tian, C., Girit, C., Zettl, A., Crommie, M., & Shen, Y. R. (2008). Gate-variable optical transitions in graphene. *science*, *320*(5873), 206-209.

Wilson, M. (2006). Electrons in atomically thin carbon sheets behave like massless particles. *Physics Today*, *59*(1), 21.

Wunsch, B., Stauber, T., Sols, F., & Guinea, F. (2006). Dynamical polarization of graphene at finite doping. *New Journal of Physics*, *8*(12), 318.

Xia, F., Mueller, T., Lin, Y. M., Valdes-Garcia, A., & Avouris, P. (2009). Ultrafast graphene photodetector. *Nature nanotechnology*, *4*(12), 839-843.

Xu, C., Jin, Y., Yang, L., Yang, J., & Jiang, X. (2012). Characteristics of electro-refractive modulating based on Graphene-Oxide-Silicon waveguide.*Optics express*, *20*(20), 22398-22405.

Xu, K., Cao, P., & Heath, J. R. (2009). Scanning tunneling microscopy characterization of the electrical properties of wrinkles in exfoliated graphene monolayers. *Nano letters*, *9*(12), 4446-4451.

Yan, H., Li, X., Chandra, B., Tulevski, G., Wu, Y., Freitag, M., et al. (2012). Tunable infrared plasmonic devices using graphene/insulator stacks.*Nature Nanotechnology*, *7*(5), 330-334.

Yu, X. (2013). *FDTD Modeling of Graphene-Based RF Devices: Fundamental Aspects and Applications* (Doctoral dissertation, University of Toronto).

Zhang, Y., Tan, Y. W., Stormer, H. L., & Kim, P. (2005). Experimental observation of the quantum Hall effect and Berry's phase in graphene. *Nature*,*438*(7065), 201-204.